nature reviews methods primers

https://doi.org/10.1038/s43586-025-00399-7

Primer

Check for updates

# In vivo microelectrode arrays for neuroscience

Nathaniel P. Williams[1,2], Mihaly Voroslakos[3], Delin Shi[1,2], May Yoon Pwint[1,2], Vittorino Lanzio[4], Hongwei Mao[2,5], Pavlo Zolotavin[6], Euisik Yoon[4,7,8,9], Thomas Stieglitz[10,11], Chong Xie[6,12,13], Timothy D. Harris[14,15], Andrew B. Schwartz[1,2,5] & Xinyan Tracy Cui[1,2]

## Abstract

Microelectrode arrays (MEAs) are devices capable of recording extracellular action potentials (spikes) from many neurons simultaneously and with high spatial and temporal resolution. MEAs have emerged as an invaluable tool for understanding how networks of neurons govern complex sensory, motor and decision-making processes. In this Primer, we introduce various in vivo MEA designs and describe their construction, characterization and applications. We describe approaches for effective device implantation and the use of MEA recordings in behavioural experiments. We then discuss strategies for obtaining high-quality and stable electrophysiological recordings, including through mitigating the foreign body reaction. We introduce the reader to spike sorting approaches with a focus on semi-automated sorting of high-channel-count data, as well as to the analysis of sorted spikes and their uses. Finally, we cover future trends and emerging MEA technology designed to expand current capabilities and overcome limitations, with a focus on biomimetic and multifunctional devices. This Primer should provide the reader with a foundation in the fundamental principles of MEA technology for in vivo use.

## Sections



[1]Department of Bioengineering, University of Pittsburgh, Pittsburgh, PA, USA. [2]Center for the Neural Basis of Cognition, Pittsburgh, PA, USA. [3]Neuroscience Institute and Department of Neurology, NYU Grossman School of Medicine, New York University, New York, NY, USA. [4]Department of Electrical Engineering and Computer Science, University of Michigan, Ann Arbor, MI, USA. [5]Systems Neuroscience Center, University of Pittsburgh, Pittsburgh, PA, USA. [6]Department of Electrical and Computer Engineering, Rice University, Houston, TX, USA. [7]Department of Biomedical Engineering, University of Michigan, Ann Arbor, MI, USA. [8]Department of Mechanical Engineering, University of Michigan, Ann Arbor, MI, USA. [9]Center for Nanomedicine, Institute for Basic Science (IBS), Yonsei University, Seoul, Republic of Korea. [10]Laboratory for Biomedical Microtechnology, Department of Microsystems Engineering-IMTEK, University of Freiburg, Freiburg, Germany. [11]BrainLinks-BrainTools, University of Freiburg, Freiburg, Germany. [12]Rice Neuroengineering Initiative, Rice University, Houston, TX, USA. [13]Department of Bioengineering, Rice University, Houston, TX, USA. [14]Janelia Research Campus, Howard Hughes Medical Institute, Ashburn, VA, USA. [15]Department of Biomedical Engineering, Johns Hopkins University, Baltimore, MD, USA.
e-mail: xic11@pitt.edu

## Introduction

Neuronal cells have a highly dynamic membrane potential and produce action potentials that can be measured using electrodes placed nearby and coupled to amplifiers and recording instruments. These measurements of the activity of neural tissue can be used to elucidate how the nervous system coordinates bodily functioning and generates sensation, decision, action and emotion. Neural tissue can also be excited through charge injection by electrodes. The combination of these tools has great potential for understanding and treating neuropathological conditions and for restoring lost neural function in both preclinical and clinical settings.

There are many different forms of electrodes and electrode arrays for recording and stimulating neural activity in vivo. Electrodes can be classified by how they interface with the nervous tissue, as surface, intracortical or intraneural, as well as whether their intended anatomical targets are part of the central or peripheral nervous system (PNS). They can also be classified by size, where macroelectrodes have a geometric surface area of >10,000 $\mu m^2$ and microelectrodes <10,000 $\mu m^2$. Microelectrodes can again be subdivided into single microelectrodes and microelectrode arrays (MEAs)[1]. In this Primer, we focus on the use of intracortical and intraneural MEAs in vivo and what they can achieve. MEAs are typically designed to be used in mammalian model organisms such as rodents, swine and non-human primates.

An MEA consists of a single integrated device containing independent electrically isolated and individually addressable microelectrodes, each capable of recording electrical signals from one or a group of neurons. MEAs can vary from 10 to more than 1,000 electrodes and generally include a component for connecting the microelectrodes to equipment for amplifying, digitizing, storing and processing signals. This is commonly referred to as a backend, or headstage when the MEA is mounted to the head. Compared with other modalities for measuring neuronal activity such as macroelectrodes, functional MRI, functional near-infrared spectroscopy, electroencephalography, electrocorticography and fluorescent $Ca^{2+}$ imaging, MEAs give comparatively high spatiotemporal specificity and good signal-to-noise ratio (SNR) and, unlike other methods, enable the sampling of action potentials from individual neurons under proper experimental conditions. By contrast, macroelectrodes only access the aggregate signal from many neurons, a measurement known as local field potential (LFP). The increasingly high electrode density and optimization of the spatial arrangement and dimensional topology of modern MEAs allow sampling of a large number of neurons across multiple areas and multiple layers of nervous tissue, with information about the relative locations of neurons inferred based on the geometry of the MEA. This makes MEAs a uniquely powerful tool for understanding the complex functions of neuronal ensembles (Box 1).

The mechanical and electrical properties of MEAs can be defined during fabrication, giving rise to a large design space that has yet to be fully explored. This has led to a proliferation of new MEA geometries suited to particular anatomical targets and refinements for improving performance, such as mechanically flexible MEAs and surface modifications to improve tissue integration, electrode coatings to increase SNR and the integration of optogenetic capabilities via micro-light-emitting diodes (µLEDs). These advancements are improving the longevity and stability of neural recordings as well as the number of neurons recorded and are essential for performing complex in vivo recording and stimulation experiments to elucidate the neural underpinnings of sensation and action (for examples of scientific questions that can be addressed, see the 'Applications' section). MEAs have been used in vitro for recording from and stimulating brain slices, ex vivo retina, nerve models, organoids and cultured neurons[2–4]. Chronically implanted MEAs have successfully been used for implantable brain–computer interfaces (BCIs) and brain–machine interfaces[5,6] to control cursor movements[7,8] and robotic prostheses[9,10], a system being explored as treatments for paralysis after spinal cord injury and stroke[11]. MEAs are also being investigated for speech decoding[12,13], tactile feedback[14] and restoration of hearing and sight[15,16]. Further applications of MEAs outside the nervous system include electrical recording and stimulation of cardiac tissue[17–19], skeletal and smooth muscle[20,21]. In fibroblasts and endothelial cells, electrical stimulation has been shown to influence cell migration and wound healing[22].

MEAs fall into several broad categories based on their materials and construction. Different MEA designs are available off-the-shelf from neurotech research companies. Many research laboratories also custom-fabricate or modify existing MEAs to suit the needs of their particular experiments or to test the efficacy of novel designs. The most common types of MEAs are silicon arrays, complementary metal–oxide–semiconductor (CMOS)-integrated arrays, flexible arrays and microfibre and microwire arrays (Fig. 1).

### Box 1 | Advantages of simultaneous multichannel recordings

Much foundational neuroscience in the early part of the twentieth century was accomplished using only single microelectrodes, made by electrochemically sharpening thin wires and drawing glass pipettes[355,356]. Continued technological development has led to microelectrode arrays (MEAs) with increasing numbers of recording channels on a single device. This makes it possible to record action potentials from multiple individual neurons and to sample the rich spatiotemporal dynamics of neuronal networks. The benefits of MEA recording also include a higher data collection rate and online decoding of accurate neural representations, which is necessary for the design of closed-loop experiments in which the responses of neurons influence the conditions of the experiment, as well as the online control necessary for biomedical applications. MEA recordings also allow for the synchronous determination of both the spatial and temporal distribution of responses, allowing for a more accurate mapping between how neurons are distributed in the tissue and how they process information[357]. Importantly, this can be used to gather direct evidence for the interconnectedness of neurons and neural populations and how this links to behaviour[358,359]. The tuning functions of individual neurons are noisy and can rarely be used to unambiguously transform firing rate or firing time to encoded variables. Responses of multiple simultaneously recorded neurons are required to remove such ambiguity. For example, in a centre-out reach task, a motor neuron that is best activated by a reach +90° from anterior body orientation might have roughly equivalent responses to a +45° and a +135° reach; therefore, simultaneous recording from additional neurons with different preferred tuning directions is usually necessary to unambiguously decode movement direction. In studies that involve multiple external variables with high degrees of freedom (such as joint angle, motion speed or force), recordings from a group of neurons with various receptive fields are necessary.

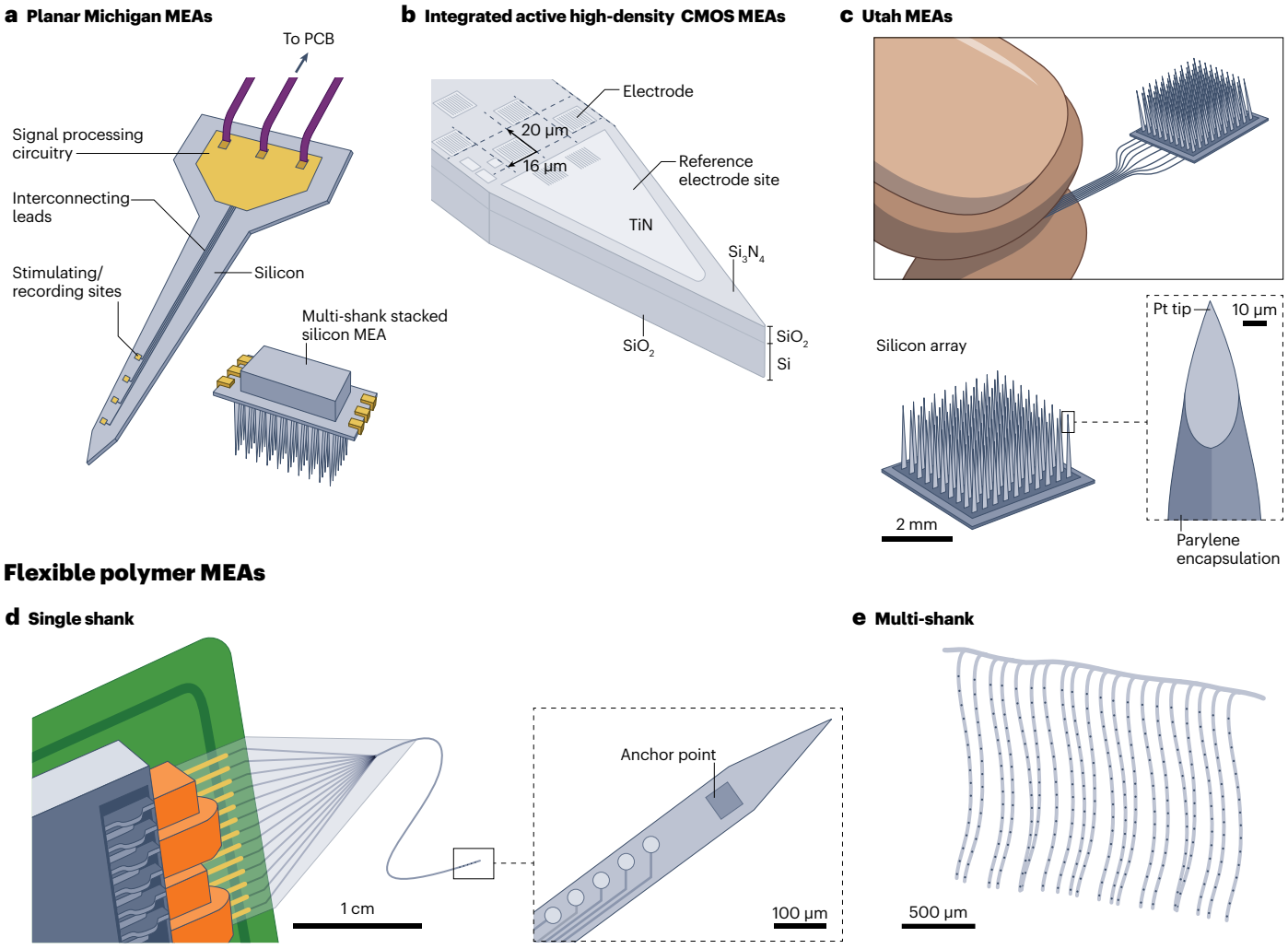


**Fig. 1 | Types of microelectrode arrays. a**, Schematic of a single-shank silicon planar microelectrode array (MEA). Bottom right: schematic of a multi-shank stacked silicon MEA. **b**, Schematic of a high-density array with complementary metal–oxide–semiconductor (CMOS) integration pre-fabricated underneath the recording sites. Fabricated from silicon oxide on a silicon wafer with a silicon nitride top insulation layer and titanium nitride microelectrode sites and reference electrode[35]. **c**, Schematic of a Utah silicon MEA. Inset shows a single shank with the de-insulated platinum tip and parylene insulation layer. **d**, Schematic of a flexible polymer MEA attached to a printed circuit board (PCB). Inset shows the probe shank with a hole for anchoring a temporary insertion shuttle. **e**, Schematic of a multi-shank flexible polymer MEA. Dark spots are individual electrode sites. Part **a** adapted with permission from ref. 38, IEEE. Part **a** inset adapted with permission from ref. 347, IEEE. Part **c** adapted with per mission from ref. 236, IOP.

In this Primer, we focus on the in vivo use of MEAs for basic neuroscience. We give an overview of MEA components, common MEA designs and their basic materials and construction process as well as some application-specific design considerations. We discuss criteria for selecting an appropriate MEA design based on the experimental paradigm. We then cover the development of new MEA technology, allowing an increase in the number and types of signals that can be recorded, a reduction in the foreign body response (FBR) and an increase in the functional lifetime of chronically implanted MEAs. This Primer provides a broad overview for those seeking a better practical understanding of MEAs for in vivo use. For other uses of MEAs, we refer readers to comprehensive reviews summarizing in vitro[23,24] and clinical[25] applications. For in-depth reviews of larger electrode technologies such as electrocorticography, deep brain stimulation and non-electrical neural recording such as two-photon $Ca^{2+}$ imaging, see referenced works[26–29].

## Experimentation

### Materials for MEAs

A typical MEA consists of several components. MEAs are generally constructed on a substrate, typically a commercially available silicon wafer. The electrode sites interface with the tissue and the signal is carried through the MEA via fine conductive interconnects — also known as traces — to external equipment. The interconnects are surrounded

by an insulator (sometimes referred to as a dielectric material), which blocks conduction between traces to minimize crosstalk and blocks conduction between traces and the tissue to reduce biological noise and prevent the traces reacting with the tissue chemically[30]. The interconnects terminate at pads that connect to a small printed circuit board (PCB), which is connected to a headstage through conventional pin-style plug connectors. In some designs, the headstage is integrated directly into the PCB. Pre-amplification is performed on the headstage (or in the case of CMOS arrays, on the MEA itself) and the signal is then transmitted to amplifiers and data acquisition systems through conventional wires. We describe these components subsequently.

**Insulation materials.** Insulation materials can be either inorganic or polymeric. The most used inorganic materials are silicon dioxide, silicon nitride and silicon carbide; polymeric materials include SU-8, parylene-C and polyimide[31]. Silicon-based MEAs often use inorganic insulators, whereas flexible MEAs use polymeric insulation. When choosing an insulation material for in vivo MEAs, it is vital to choose materials that provide both the desired mechanical properties: adhesion to other layers (insulation and traces) and longevity (low moisture uptake, high biocompatibility and low dissolution rate)[32].

**Conduction material for traces and electrodes.** Several conductive materials are used in the construction of MEAs, often with different materials chosen for traces and electrodes[33]. Typically, traces are made of thin conductive layers (<200 nm) integrated with a thin adhesion layer (<20 nm of either titanium or chromium). CMOS arrays integrate aluminium–copper traces into six metal layers to form the CMOS on-probe circuitry[34,35]. Electrode materials are chosen based on adhesion to the substrate, biocompatibility, conductivity, conduction mechanics (ionic or electronic), charge transfer mechanics, charge storage capacity, charge injection limit (also referred to as charge injection capacity) and stability. Typical electrode materials include gold, platinum, iridium and indium tin oxide. Smooth microelectrodes often have relatively high impedance (>1 MOhm at 1 kHz) as a lack of surface roughness results in a low electrochemical surface area. To increase the electrochemical surface area and improve electrochemical properties, the electrode site can be coated with materials such as iridium oxide, titanium nitride, metal nanoparticles and conducting polymers during or after fabrication[36,37] (Supplementary Note 1).

## Types of MEAs

**Silicon arrays.** Planar silicon MEAs (Fig. 1a), commonly referred to as Michigan style arrays as they originated from the University of Michigan, are microfabricated on silicon wafers[38,39]. This process allows for high-density electrode integration and flexibility in terms of size, spacing and configuration of electrode sites on the MEAs along with circuit integration on the same chip. Planar silicon MEAs comprise two main areas: a narrow shank (5–10 mm long by 50–100 µm wide and 20 µm thick) that contains the microelectrode sites, and a wider backend area, typically a few millimetres wide, containing circuits (in some cases) and contact pads for connection to a PCB. Each contact pad is connected to an electrode through a microfabricated metal trace (typically 0.2–2 µm wide). Early devices used multiple electrodes along one or more silicon shanks without active electronics for on-chip signal processing (passive MEAs), but as the number of recording sites increased to more than 100, active circuits were integrated at the backend[40,41]. This approach was then expanded to 3D configurations[42] (Fig. 1a, inset), in which multiple 2D arrays were stacked onto each other to allow for 3D spatial arrangement and sampling.

Recently, active electronics (for example, CMOS) integrated onto silicon MEAs have become available[34,40,41,43–46] (Fig. 1b). CMOS circuits contain the amplifiers, filters, multiplexers and digitizers necessary for a recording system fabricated directly into the MEA shank itself beneath the electrode sites. These active electronics comprise the application-specific integrated circuit. CMOS integration allows for switching between multiple sites sharing a single trace using time-division multiplexing (as in SiNAPS probes distributed by Plexon Inc. and NeuroNexus Technology) or by static switching and pooling (as in Neuropixels)[47]. This greatly reduces the footprint of the probe, the interconnect and PCB dimensions compared with passive probes with a dedicated trace for each electrode. This increase in the number of electrodes for a given tissue volume improves sampling density in both acute and freely behaving experiments[40,44,48–50].

Another type of silicon MEA is obtained by dicing and etching electrode pillars directly through silicon[51,52] and is often referred to as a Utah-style array (Fig. 1c). These bed-of-nails style arrays are limited in shank depth and typically constrained to a single electrode per shank. Standard Utah arrays consist of a 10-by-10 grid of 1 mm-long shanks, with 400 µm shank spacing. Utah arrays have been used in humans to record from the motor cortex and stimulate the somatosensory cortex for BCI medical applications[53,54]. Alternative fabrication approaches to create bed-of-nails style arrays with greater electrode density and channel count are currently being explored; these include 3D printing, two-photon polymerization and deep reactive-ion etching[55–57].

**Flexible arrays.** Flexible arrays (Fig. 1d) were developed in an effort to improve the tissue integration, longevity and reliability of MEAs[58,59]. Flexible arrays are microfabricated in a similar manner to planar silicon arrays at similar dimensions; however, they make use of soft and flexible insulation and thin conductive traces. Once fabricated, these arrays are released from a carrier wafer, resulting in thin (1–20 µm) shanks that can flex in response to tissue micromotion, thereby reducing mechanical-mismatch-induced tissue damage and inflammation. An alternative approach to integrating CMOS directly onto the MEA, as described earlier, consists of the hybrid integration of MEAs onto a separate CMOS circuit (typically on the headstage), which decreases headstage dimensions and allows for greater flexibility regarding the choice of MEA materials and technologies. Flexible arrays, for instance, can be hybrid-integrated onto CMOS circuits[60]. Flexible arrays can also be fabricated in multi-shank designs and assembled into 3D configurations[61–64] (Fig. 1e).

**Fibre and wire arrays.** Additional types of MEAs include microwire and carbon fibre brush arrays and multifunctional fibres, which are made into arrays by bundling insulated microwires or carbon fibres or by extruding fibre preforms[65–67]. These devices generally have lower fabrication cost and complexity than other forms of MEAs; however, scaling to dozens or hundreds of sites is challenging and the determination of the relative positions of the sites tends to be less precise owing to splaying of wires during insertion. For more in-depth reviews of fibre and wire arrays, see refs. 68–72.

## Use of MEAs for neural stimulation

MEAs can be used for electrical stimulation of neurons, which when combined with recording and behavioural studies can be a powerful tool for inferring the function of particular groups of neurons.

## Box 2 | Optoelectrodes

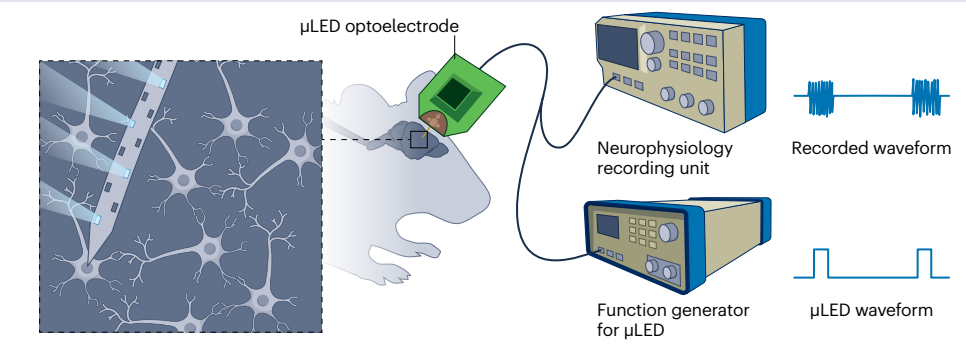


The desire to perform optogenetic stimulation during neural recording — the activation of neurons with light using light-sensitive ion channels transgenically expressed in the target cells[360] — resulted in the development of several silicon and complementary metal–oxide–semiconductor[361] optoelectrodes integrating optical fibres, waveguides[361–366] or micro-light-emitting diodes (μLEDs)[225,367,368] (see the figure). Optical fibres can be directly attached onto a passive or active silicon probe shank; however, this increases the implant size and restricts illumination to large neural populations. Waveguides and μLEDs monolithically integrated onto microelectrode arrays allow for spatially confining the illumination to one or few neurons in selectable sites along the shank[361–370]. Waveguide approaches typically integrate a single-input waveguide in the probe coupled to an external laser source through an optical fibre. For multisite illumination, silicon nitride waveguides embedded in silicon dioxide direct light to different waveguide outputs along the shank or allow steering of the beam output angle[362] using either external laser wavelength tuning[365,371] or by the integration of optical switches[361,369]. Waveguides for flexible arrays have been demonstrated using polymeric materials such as SU-8 and ormocers[370], but have not shown optical switching capabilities. Probes monolithically integrating μLEDs allow for optical site selection by applying an electrical current through the μLED mesa. For example, blue μLEDs are made of layers of indium gallium nitride and are patterned in small dimensions (~8×11 $\mu m^2$)[225,367,368]. Although optoelectrodes integrating waveguides require complex assembly steps such as fibre-to-waveguide alignment and gluing, optoelectrodes integrating μLEDs only require electrical connection using the same packaging techniques used for recording arrays (such as wire bonding, microflex interconnect[372] or flip chip bonding). These devices have allowed much greater ease and flexibility in combining electrophysiology with optogenetics in a small form factor while minimizing tissue disruption. Several recording probe companies (such as Neuronexus and Cambridge Neurotech) provide the option of fibre attachment to silicon recording probes. Neurolight Technologies offers optoelectrodes integrating μLEDs. Neuron waveform adapted from ref. 373, Springer Nature Limited.

The location and shape of the electrodes affect the activation volume. Charge transfer characteristics can be enhanced by using rough or porous materials to increase the electrochemical surface area[73] or by making electrodes from materials capable of reversible oxidation such as iridium oxide or polyethylenedioxythiophene (PEDOT)[74–76]. See Supplementary Note 1 on electrode surface modification for details. Additional considerations for stimulating electrodes include electrically induced mechanical nano-oscillations, which could lead to mechanical failure[77]. This physical response should be taken into account when designing MEAs for stimulation. MEAs containing optical components, referred to as optoelectrodes, can be used to stimulate cells optogenetically; this can give greater cell-type specificity than electrical stimulation. For details on optoelectrodes, see Box 2.

**Acute and chronic preparations.** In the context of in vivo MEA experiments, an acute preparation is one in which electrodes are not fixed to the skull but inserted for each experimental session, lasting from a few hours to a day at most in rodents or several days at most in large animal models[78,79]. The animal is either kept under anaesthesia for the duration and euthanized at the end of the experiment[80] or the craniotomies are covered and the animal allowed to recover, whereby multiple sessions can be performed in an awake head-restrained animal. In a chronic preparation, the animal is allowed to recover following surgery and experiments are carried out over days, weeks, months or years[81]. Animals are either anaesthetized or awake during experimental sessions and allowed to behave freely in their home environment otherwise. Chronic studies are necessary to observe long-term neuronal changes such as learning, memory or disease progression. Some studies with time endpoints in the range of a few weeks are referred to as subchronic or semichronic[82–84]. Under anaesthesia, studying complex behaviour is not possible, although many sensory and reflexive responses remain intact under proper anaesthetic conditions[85,86].

All MEA types can be used for acute recordings. The main advantage of acute paradigms is a simplified surgical approach, allowing greater access to anatomical targets, more convenient implanting of multiple MEAs to study multiregion neuronal activity[87–89] and, for anaesthetized preparations, the ability to administer many more stimulus conditions in a single session than would be feasible in an awake-behaving experiment. Acute preparations eliminate constraints on the size and weight of the experimental set-up as components do not need to be carried by the animal and can be held by external supports. Motion artefacts can be reduced under anaesthesia; however, the effect of anaesthetics on neural dynamics must be considered – for a review of these effects, see ref. 90.

Chronically implanted arrays are necessary for investigating natural movement, perception, learning and memory, decision-making and social interactions. In chronic experiments, MEAs are fixed to the skull with dental cement[91] and therefore must be light and compact enough for the animal to carry, as well as reliable for long-term use. The headstage required could vary depending on whether recording,

stimulation or both are performed. Headstages contain microelectronics such as pre-amplifiers and are designed to interface with a specific hardware and software ecosystem; therefore, the connectors and instrumentation should be considered together when designing experiments.

Chronic experiments must contend with the FBR, which can cause glial encapsulation and neuronal degeneration in the vicinity of the implant, increasing the impedance of recordings and decreasing signal quality. One way to mitigate this is to use a microdrive to allow advancement through the tissue after implantation[92–99] and precise positioning within the brain tissue. Gradual penetration through the target region allows sampling of new neurons each day and recording signals unimpeded by the formation of glial encapsulation. Floating arrays that are not fixed to the skull can also be used to reduce glial encapsulation by reducing the effect of micromotion of the array relative to the moving brain[100–103]. For a more detailed description of the FBR and strategies to mitigate its negative effects on MEA performance, see the section 'Biocompatibility'.

## Electrode design considerations

There remain questions as to whether the size, material or impedance of an electrode is the essential parameter necessary to obtain optimal recordings. For a given material, larger electrodes generally have lower impedance and a higher SNR. They record LFPs well but are not able to discriminate single-unit activity (SUA) as the electrical potentials from many neurons are integrated over the large electrode site. Smaller electrodes are better for single-unit discrimination. The transfer impedance, more than the material itself, determines the signal quality; the lower the impedance, the lower the thermal noise and the higher the SNR. Therefore, low-impedance electrode coatings on small sites are a good approach for high single-unit discrimination and high SNR[104]. The size and location of the electrode sites — whether they are at the tip, edge or centre of the shank — determine the listening volume — the volume of tissue that a given electrode samples from. An ideal MEA has a small footprint and many electrodes, and recent advances in MEA technology have made it possible to meet these competing requirements and to record hundreds or even thousands of neurons from a single head-fixed awake[48,49] or freely moving animal[51,105,106].

**Considerations for experiments in the peripheral nervous system.** Most peripheral nerves contain multiple functionally grouped fascicles of afferent and efferent fibres, with more fascicles proximal to the central nervous system (CNS) and fewer distally. Therefore, target selection is a trade-off between having access to many fascicles with efferent and afferent connections to more of the body (close to the CNS) and being able to specifically access only a small number of fascicles with efferent and afferent connections only to a restricted part of the body (farther from the CNS). Targeting more peripheral fascicles could minimize potential off-target effects from stimulating or recording fascicles that are not of interest. Across species, peripheral nerve diameter varies between ~100 µm up to ~10 mm and the number of fascicles varies from single digits up to several dozens. It is therefore difficult to give a general recommendation for a specific nerve interface. In general, the size of the target nerve, the number of fascicles and anatomical access must be balanced against the desired spatial selectivity for recording and stimulation. Surface electrodes, the least invasive measurement approach, provide low specificity compared with intraneural electrodes, whereas coverage of a whole nerve can be achieved with a circumferential cuff electrode and activation or recording from a few fibres requires an intrafascicular approach. A high-channel-count MEA such as a bed-of-nails or thread with embedded electrode sites is required to cover the whole nerve diameter at high resolution[107]. In the case of bioelectronic medicine for the control of neuroprosthetics, distal branches are often selected to maintain specificity[107].

The need to selectively stimulate afferent or efferent or large or small fibres influences the choice of device. Cuff electrodes with asymmetric electrode and current source arrangements have been used for fibre-specific stimulation; however, in this set-up, the lower excitation threshold of large fibres means that these are driven into their refractory phase by subthreshold pulses before small fibres are activated[108]. This differs from physiological conditions in which thin fibres are activated first. Exogenous electrical stimulation recruits larger axons first owing to their larger surface area and lower resistance to electrical currents. Additionally, for myelinated axons, larger axons have a longer distance between nodes of Ranvier (myelin sheath gaps — the excitable portion of the axon), which means that for the same amount of charge injection, a larger potential difference is generated between different nodes, thus causing the activation threshold to be reached sooner than in smaller axons. An approach using multiple electrodes in one cuff to adjust the potential based on the distance between nodes in different fibre types to preferentially activate small fibres has been proposed[109], although adoption of this approach has been limited so far. Cuff electrodes have limited spatial selectivity, although multiple channels and the spatial filtering properties of the nerve allow for fascicular specificity. Intraneural MEAs are smaller and placed within the fascicle, allowing for higher spatial resolution[110,111]. However, arrays in the PNS lack stable anchor points owing to the soft-tissue environment. Anchoring a connector on the skull and subcutaneously routing cables to the MEA in the periphery have been performed in rodents to circumvent this issue[112], although this approach can be prone to detachment problems in large animal models.

## MEA fabrication

Fabrication steps vary somewhat among manufacturers, laboratories and device configurations. The general steps for the major array types are outlined here as an introduction for those interested in custom probe design and as background for end users to better understand the devices they will be working with.

**Silicon.** Planar arrays are batch-fabricated on doped silicon or silicon-on-insulator wafers. First, an initial insulation layer is deposited, often silicon oxide. Traces are then patterned using high-resolution lithography techniques (typically optical lithography or electron beam lithography for traces <200 nm in width). Smaller traces allow for accommodating more electrodes per shank. Electrodes are patterned following the addition of another insulation layer and contact via opening to remove insulation from traces at electrode sites and contact pads, necessary to ensure good electrical continuity. Next, the passivation layers and a few tens of micrometres of silicon are etched around the array to define its outline. The final process is the etching or thinning of silicon from the wafer backside by deep reactive ion etching, up to the frontside trench depth, releasing the arrays from the wafer (Fig. 2a).

Once fabricated, arrays are assembled onto a PCB. The bonding pads of the array are electrically connected to each corresponding PCB pad by wire bonding, flip chip bonding or a microflex interconnect[38,113]. The fabrication of Utah silicon arrays differs from that of planar arrays primarily in that the silicon substrate is either machined or deep etched to

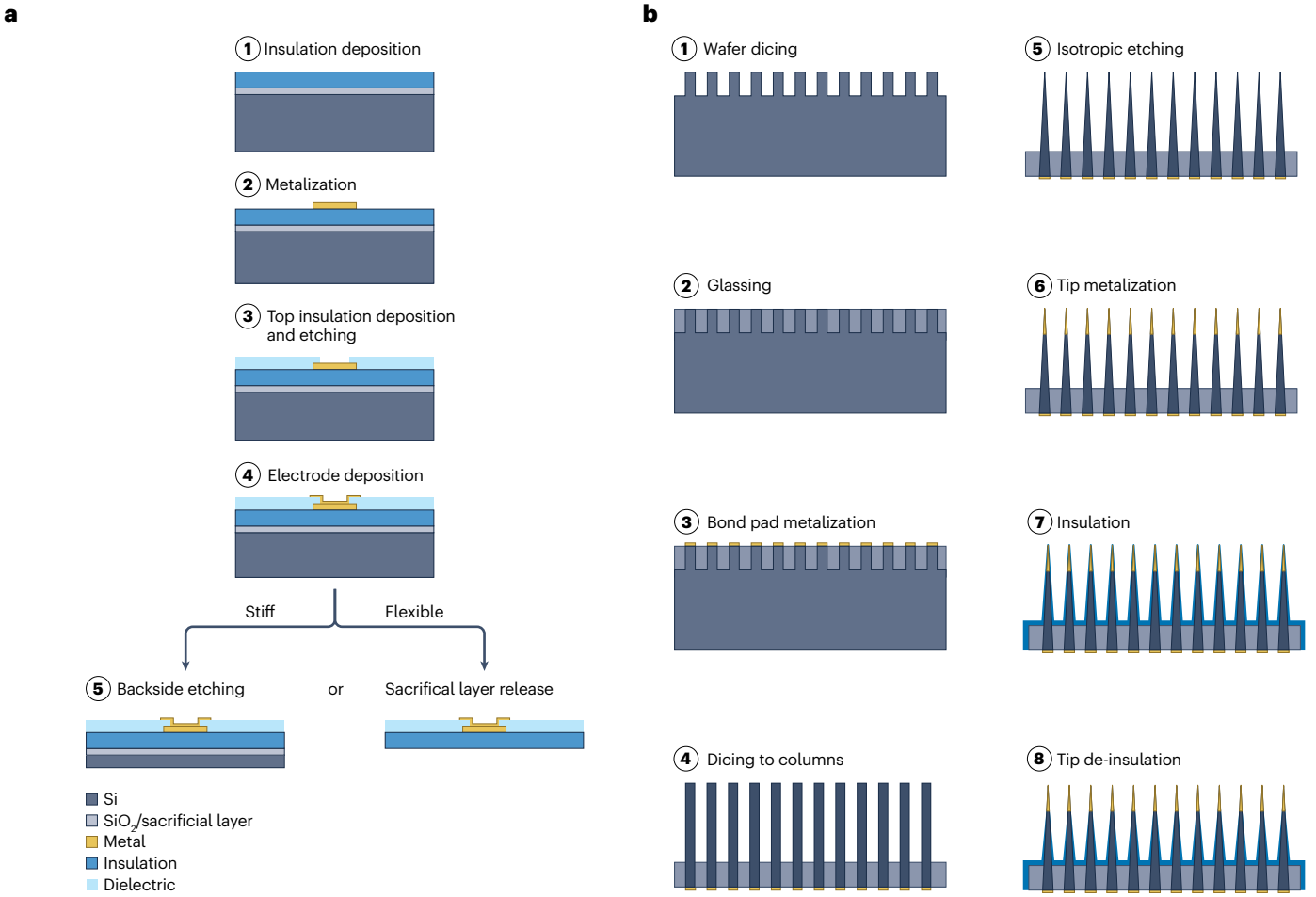


**Fig. 2 | Schematic of the fabrication process. a**, Schematic of the general fabrication process for planar microelectrode arrays (MEAs). The overall process is similar for rigid and flexible arrays, the differences being that flexible MEAs use flexible materials and are released by etching away a sacrificial layer or lifted off the solid substrate rather than etching through the wafer. For planar arrays of both types, lithography and other high-resolution fabrication processes are used to create an initial insulation layer (1) followed by patterning of interconnecting lines (2) sandwiched between insulation layers. Insulation layers are selectively etched to expose electrical contact areas on the traces (3) before the deposition of metal electrodes (4). Finally, the sacrificial layer is etched away (flexible) or the silicon substrate is etched through (stiff) to release them (5). **b**, Schematic of the general fabrication process for Utah MEAs. A thicker silicon wafer is used than for planar arrays (larger than the desired length of the electrode shanks). The silicon wafer is diced and then filled in with glass (1 and 2) to form the base insulation. As an alternative to step 2, thermomigration on a non-conductive wafer can be used to create individually insulated conductive pillars before contact pad deposition (3). The following steps include further dicing (4), etching (5) metal deposition on the electrode tips (6), top layer insulation (7) and finally tip de-insulation (8).

form electrode site pillars[51,52] (Fig. 2b). Typically, all shanks are the same length, although Utah arrays with variable shank length can be made by adding an additional variable-height dicing step[114]. In CMOS arrays, which differ from passive silicon arrays, the CMOS-integrated circuit is first fabricated onto silicon-on-insulator wafers (Fig. 1b); these wafers have a top silicon substrate and a buried oxide layer below this substrate. On top of the CMOS device layer, all of the interconnects and insulation are patterned in the same manner as other planar silicon devices[43,115,116].

**Flexible polymer thin film.** The fabrication process for flexible arrays[117] shares some similarities with conventional silicon arrays as it too relies on techniques developed for microelectromechanical devices. Glass or doped silicon wafers are used as a substrate. To facilitate the full or partial release of MEAs from the wafer, a thin sacrificial metal layer such as nickel, aluminium or chromium is typically defined before the deposition of any MEA material. A polymer material is then deposited via spin coating or vapour deposition to form a bottom insulation layer. Next, metal is deposited by evaporation or sputtering and lithographically patterned to form interconnects between future electrode sites and backend connectors. A top polymer insulation layer is then deposited. Steps for interconnect lines and polymer insulation deposition can be repeated multiple times to achieve vertically stacked, high-density MEAs. The polymer is then etched to open vias to the interconnects (traces) for subsequent electrode deposition as well as to define the probe outline, similar to the process for silicon MEAs (Fig. 2a). MEAs are released by etching away the sacrificial layer. Thicker arrays can be released from the wafer by peeling after a hot water bath or laser ablation.

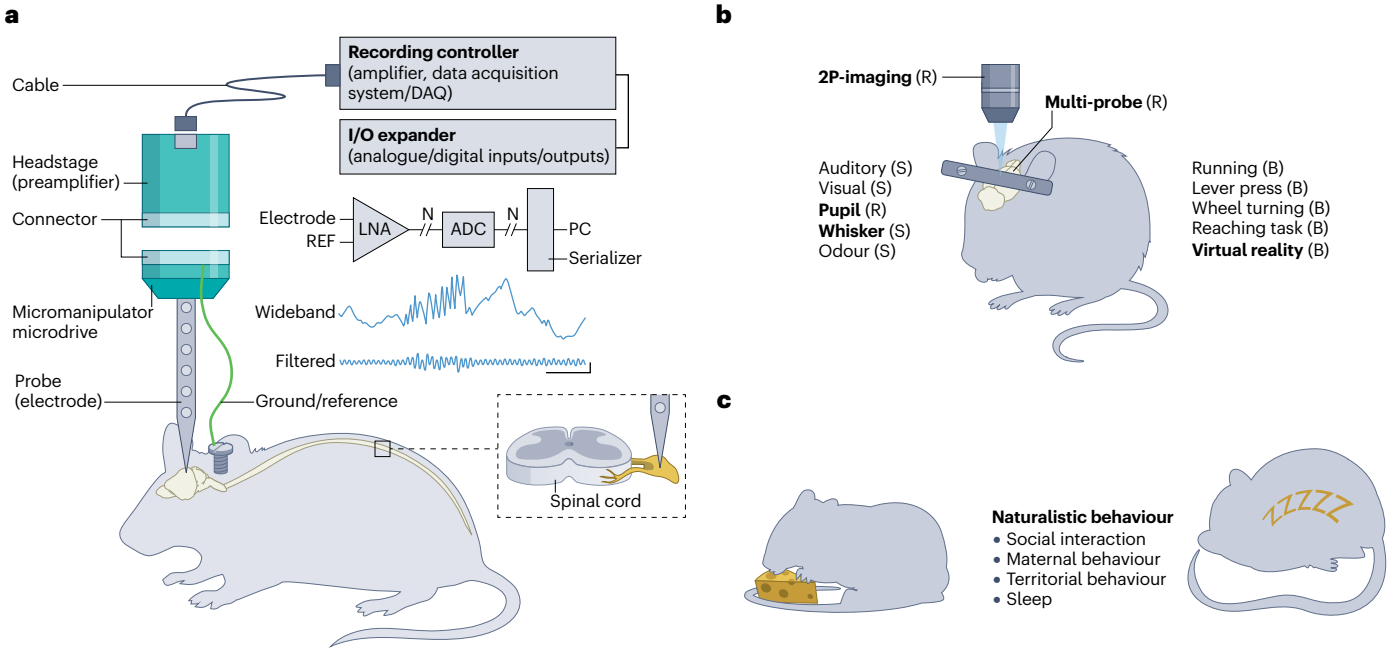


**Fig. 3 | In vivo experimental set-up. a**, Microelectrode arrays (MEAs) are used to record local field potential and action potential signals from the central nervous system or peripheral nervous system (blue traces, scale bar, 50 ms, 100 µV). MEAs often use a bone screw as a reference (REF) and ground electrode or contain an internal reference. A pre-amplifier is connected to the MEA. The signal is sent through neutral (N) wires, amplified by a low noise amplifier (LNA), digitized by an analogue-to-digital converter (ADC), serialized in the pre-amplifier and either recorded with a recording controller containing an amplifier and data acquisition system (DAQ) connected to a computer (PC) or saved to onboard flash memory in a wireless system. Analogue and digital signals can be connected to an input/output (I/O) expander to synchronize multiple data streams with electrophysiology. **b**,**c**, MEAs can be used in either head-fixed (part **b**) or freely moving (part **c**) animals. **b**, Head-fixed preparation allows recording (R) or stimulation (S) during behaviour (B) using modalities that are challenging in freely moving animals (these modalities are in bold). It also allows combined electrophysiology and imaging — for example, using two-photon (2P) systems — or to record with multiple MEAs (typically more than four devices). **c**, Chronic recordings in freely moving animals allow the collection of neuronal data in naturalistic behaviours such as social interaction, open exploration and natural sleep.

## Electrophysiology data collection

MEAs can record action potentials as well as LFPs[118]. Action potentials represent the activity of a single neuron and have an amplitude of a few hundred microvolts and a frequency range (or bandwidth) of 300–10,000 Hz (ref. 119). Action potential signals last ~1 ms, whereas the majority of LFP signals fluctuate on the order of tens of milliseconds or slower. LFPs comprise the aggregate signal across a large volume of tissues — hundreds of microns to millimetres — and represent the combined activity of hundreds of neurons within that volume. They have amplitudes from hundreds of microvolts to a few millivolts[119].

MEAs are connected to AC-coupled amplifiers, followed by an analogue multiplexer and an analogue-to-digital converter. These components are referred to as an analogue front end and are often integrated into the headstage[120]. At the interface between the recording site and the tissue, electrochemical effects can induce large direct current offsets (also known as 'bias'). To counter this, high-pass filtering is built into the design of extracellular electrophysiology amplifiers, which have bandwidths ranging from 0.1 kHz to 10 kHz (ref. 121). The analogue-to-digital converter must be able to capture both action potential and LFP signals with a sufficient SNR (>60 dB) across the full bandwidth. The sampling frequency for these wideband signals is typically 10–30 kHz (Fig. 3a). The signal is then further amplified and stored by the data acquisition system; the final step is typically performed by specialized software running on a standard desktop computer.

## Behavioural data collection

Recording is often combined with behavioural assays. Animals can perform sensory–motor tasks when head-fixed (Fig. 3b) or in freely moving paradigms when performing naturalistic behaviour such as nesting, social interaction, open field and marble burying (Fig. 3c). Monitoring behaviour requires recording different data types with different sampling rates (electrophysiology, video, analogue position and force sensors and stimulus triggers). Open-source platforms such as DeepLabCut[122] can be used for semi-automated quantification of position and pose. Synchronization of data streams is crucial for accurate analysis[123] and several tutorials are available for synchronizing data types[124–126]. For details on behavioural data collection in large animals, see Supplementary Note 2.

## Surgical approach

The scientific question being addressed and the experimental paradigm inform the types of MEAs that are suitable for a given application and the surgical approach that must be used. Two major considerations are the anatomical target or targets and whether an acute or chronic preparation is needed. Important points to consider for achieving optimal performance when selecting an MEA are target depth, the volume to be sampled (both dorso-ventral and medio-lateral) and the cellular density of the target region, which can vary by an order of magnitude between brain regions[127,128]. Surgical planning depends on

the animal model, target location and type of device. Achieving target specificity requires planning using an anatomical atlas, familiarity with stereotaxic coordinates and use of a stereotaxic frame[129]. Increasingly, presurgical CT, MRI or widefield imaging are being used for more precise planning. Analgesic should be administered both before and after surgery, and anaesthesia should be monitored throughout. All surgical implements should be clean and sterile, and surgery should be performed on a sterile field. Animal recovery should be closely monitored post-surgery[96,99,130,130132,133] (International Brain Laboratory Protocols). Although a full discussion of the various approaches to the implantation of MEAs is beyond the scope of this article, we provide a summary of surgical resources in Supplementary Table 1.

### Ethical considerations

Neurophysiological research in an intact organism is necessary to fully understand the working brain and nervous system. However, effort should be made to minimize the use of animal subjects and to eliminate distress. Experimenters should choose the least complex organism and use the fewest animals necessary to address the scientific question[134]. Statistical power analysis should be used for determining adequate sampling size[135–137]. All aspects of research involving vertebrate animals must be performed with the prior approval of a relevant oversight and regulatory body and should conform to their guidelines. These regulatory bodies should be the point of contact for ethical issues involving animal subjects.

## Results

The collection and storage of electrophysiological signals is only the beginning of the analysis and interpretation of neurophysiological data. The approach for a given experiment will depend on the scientific questions and the paradigm used to collect the data. Analysis is carried out using specialized software (with both proprietary and open-source options available) and often customized scripts written or adapted by the researcher for a particular experiment or paradigm. Several frameworks exist for the analysis of electrophysiological data collected via MEAs, with popular languages being MATLAB and Python[138–140]. Owing to the breadth and complexity of in vivo neuroscientific experiments, only the basics of data analysis will be touched on in this section. The following section begins with a brief description of how recorded spikes can be isolated from noise and assigned to putative neurons by various spike sorting methods. Following that, several established methods for the analysis of sorted spikes, useful for determining intrinsic and stimulus–response characteristics of neurons individually or as populations, are discussed.

### Electrophysiological data analysis

Electrophysiology data are usually divided into two broad categories: LFPs and action potentials. MEAs can record both action potentials and LFP. We focus on the analysis of action potentials as MEAs are the only technology capable of simultaneously recording large numbers of single-unit action potentials, whereas other electrode technologies such as surface macroelectrodes are capable of recording LFP. LFP is separated into frequency bands associated with different brain functions and has been reviewed elsewhere[141]. Detection of action potentials at the electrode site is an initially analogue process, only later digitized by equipment connected to the electrode site via the traces and stored for computational analysis. Neurons at varying distances from the MEA contribute to the recorded signal (Fig. 4a,b) and the combined signals from intermediate-distance neurons create a background signal, sometimes referred to as biological noise. Biological noise is greater in intensity than the electronic noise of the system and therefore even well-designed systems are limited by their signal to background (rather than signal to electronic noise). Isolation of single-neuron spike trains is a classic example of a signal processing problem dubbed the cocktail party problem in which the goal is to isolate a single source from a group of overlapping sources.

**Spike sorting.** Spike sorting aims to assign recorded spikes to distinct neurons (sometimes referred to as units) and relies on the assumption that each neuron produces distinct, stereotypical waveforms. Spikes that cannot be effectively sorted to distinct neurons are known as multi-unit activity (MUA) spikes, which have lower amplitude and consist of action potentials from multiple distant neurons. Any spike sorting pipeline has the following common operations: bandpass filtering (Fig. 4b), which involves the isolation of signals from ~500 Hz to 10 kHz; common average referencing to remove artefacts affecting many channels; spike detection, which in the simplest case is achieved using a threshold voltage; spike waveform extraction, in which the shape of each spike is extracted; dimensionality reduction, in which the waveform shape is decomposed into principal components; and clustering in a lower dimensional space, where boundaries between clusters of waveforms in principal component space are used to categorize waveforms as originating from a given neuron[142]. Independent component analysis can also be used for this purpose[143]. Clustering can be done manually or automatically, using *k*-means or other clustering algorithms (Fig. 4c). Automatic clustering can result in over-splitting or under-splitting, whereas manual clustering is labour-intensive and can be subjective; to overcome these challenges, many pipelines include a waveform similarity calculation, which clusters the characteristics of waveforms into individual pools, creating a spike time record for each neuron. A useful summary and comparison of computational strategies can be found in ref. 140.

Two popular, free and open-source data acquisition packages for high-channel-count recording are SpikeGLX and OpenEphys. The latter is a large ecosystem for various applications, whereas SpikeGLX is focused on Neuropixels data. For data collected using high-density arrays, a pipeline using waveform template matching with a subtraction method such as Kilosort[144] can result in improved spike detection and sorting. If operating correctly, waveform template subtraction can separate the signals from overlapping spikes and can outperform other sorting methods in terms of yield and accuracy owing to its ability to resolve overlapping spikes. Owing to the analogue nature of the raw signal, there will always be some spikes too low in amplitude to resolve unambiguously.

### Analysis of sorted spikes

Once spikes are assigned to neurons by the sorting algorithm, spike trains from each neuron can be analysed to determine meaningful characteristics such as firing rate, interspike interval (ISI), trough-to-peak time and autocorrelation. In addition, stimulus-triggered averaging can be performed to identify stimulus–response relationships, cross-correlation can be used to examine functional connectivity between neurons and decoding techniques can estimate information content and processing. These approaches form the core of electrophysiology analysis and when appropriately deployed provide insights into how neurons encode information, coordinate network activity and contribute to behaviours and cognitive functions, advancing our understanding of neural circuit dynamics in both normal and pathological states. We discuss these subsequently.

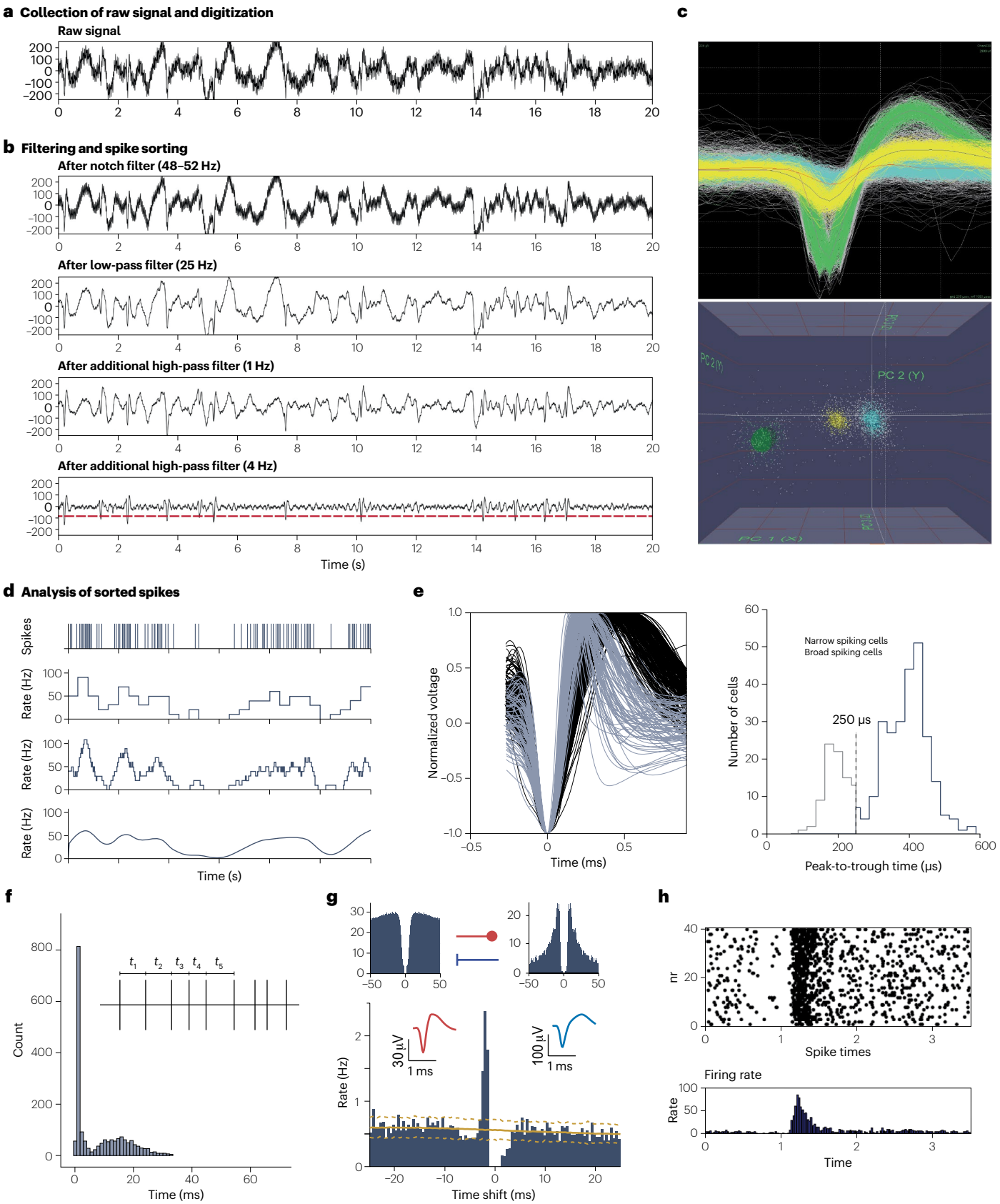
a Collection of raw signal and digitization
Raw signal
b Filtering and spike sorting
After notch filter (48–52 Hz)
After low-pass filter (25 Hz)
After additional high-pass filter (1 Hz)
After additional high-pass filter (4 Hz)
Time (s)
c
PC 2 (Y)
PC 1 (X)
d Analysis of sorted spikes
Spikes
Rate (Hz)
Time (s)
e
Normalized voltage
Time (ms)
Narrow spiking cells
Broad spiking cells
250 µs
Number of cells
Peak-to-trough time (µs)
f
Count
Time (ms)
g
Rate (Hz)
30 µV
1 ms
100 µV
1 ms
Time shift (ms)
h
Spike times
Firing rate
Rate
Time

**Fig. 4 | Spike sorting and analysis pipeline. a**, Raw signal is amplified, digitized and stored. **b**, Before spike sorting, the data are typically notch-filtered and passed through a series of low-pass and high-pass filters (the exact filtering will vary depending on the set-up used). Local field potential can also be obtained from the broadband data. For spike sorting, the high-pass-filtered data are clipped to threshold crossings, with the threshold shown by the red dashed line. *Y* axis in μV. **c**, Threshold crossings, which represent putative spikes (top), are then sorted in principal component space (bottom) based on waveform characteristics into spike clusters (putative units). Similar waveforms group together in clusters in feature space, as shown here in Plexon Offline Sorter[348]. Once spikes are sorted into units, the units can be analysed using metrics such as firing rate, trough-to-peak time and interspike interval. **d**, Firing rate. Top: threshold crossings plotted against time; second from top: histogram of data from top plotted with larger time bins; third from top: histogram of data from top plotted with smaller time bins; bottom: histogram of data from top plotted with smoothing function applied. **e**, Trough-to-peak time. Left: spike waveforms; right: a histogram of the trough-to-peak times for the waveforms shown left. **f**, Interspike interval time. **g**, Auto- and cross-correlograms. Top: auto-correlograms with average waveform shapes below. Putative excitatory connections are in red, and putative inhibitory connection in blue. Bottom: cross-correlogram for the two units shown above, plotting the influence of the putative excitatory neuron on the putative inhibitory neuron. Solid and dashed lines show the mean and 99% confidence interval of the shuffled data, as a control. **h**, Spike raster (top) of spike threshold crossings over multiple trials and peri-stimulus time histogram (bottom) of spikes shown in top. nr, number of runs (trial number). Panels **a** and **b** reprinted from ref. 349, CC BY 4.0. Panel **d** reprinted with permission from ref. 350, Association for Computing Machinery. Panel **e** adapted from refs. 349,351, CC BY 4.0. Panel **f** adapted with permission from ref. 352, The American Physiological Society. Panel **g** reprinted with permission from ref. 353, PNAS. Panel **h** adapted from refs. 349,354, CC BY 4.0.

**Firing rate.** The firing rate of a neuron is one of the most fundamental and universally applied metrics for understanding its response properties. To determine firing rate, a time window of interest is selected and the number of spikes calculated. Firing rate is typically expressed as number of spikes per second in hertz or can be displayed as a histogram with spike events binned across time. Bin size can vary and should be chosen based on the spike count statistics[145]. In some cases, firing rates are normalized to factors such as baseline activity or population averages for comparative analysis across conditions or groups. Averaging firing rates across trials provides a more robust estimate of neuronal activity (Fig. 4d). Statistical methods such as linear regression, Bayesian decoding and pairwise neuronal firing rate correlations can be applied to compare firing rates between conditions, assess changes over time or link changes in firing rates with behavioural or physiological variables[146].

**Trough-to-peak time.** Trough-to-peak time can be calculated and used to categorize neurons based on the underlying biophysical properties that give rise to their stereotyped waveform characteristics[147,148]. The trough is identified as the lowest point of the waveform, corresponding to the initial negative deflection as the neuron depolarizes, and the peak is the highest point, representing the maximum positive deflection during repolarization (Fig. 4e). Once the trough and peak are identified, the interval between them is taken as the trough-to-peak time[149]. Trough-to-peak time can give some indication of neuron phenotype; for example, short trough-to-peak times are associated with fast-spiking inhibitory interneurons in most areas of the mammalian cortex[150,151].

**Interspike interval.** ISIs provide insights into the temporal firing pattern of the neuron. Once spike times are identified, ISIs are computed as the time differences between successive spikes. ISIs are typically expressed in milliseconds and displayed as a binned histogram, as any neuron will generate a distribution of ISIs over a given period (Fig. 4f). Variations in ISI histograms can indicate burst firing (short ISIs clustered together) or regular firing (consistent ISIs over time). The minimum ISI reflects the refractory period during which the neuron cannot fire again owing to the recovery of ion channels[152].

**Correlograms.** The auto-correlogram is generated by plotting the normalized spike count of a single neuron spike train against the time lag relative to each spike and gives a representation of how spikes correlate temporally. Correlation can reveal firing patterns and temporal dynamics within a single neuron, highlighting periods of regular firing, refractory periods or burst activity. Peaks or troughs in the auto-correlogram indicate periods of increased or decreased firing rate at specific time offsets relative to each spike[142,153].

The cross-correlogram is generated by computing the correlation between the spike times of two neurons recorded simultaneously, making it possible to determine whether their firing patterns are synchronized or whether one tends to lead or lag the other (Fig. 4g). Peaks or troughs in the cross-correlogram can indicate functional connectivity between neurons, which can be either excitatory (peaks), inhibitory (troughs) or oscillatory (periodic peaks and troughs), indicating that they might be part of the same circuit or network[142,154].

**Spike raster and peri-stimulus time histogram.** Spike raster plots can visualize the timing of spikes in multiple spike trains, either from multiple neurons or across repeated trials. These plots are matrices in which each row represents a neuron or trial and each column represents a time bin. For each neuron or trial, spike times are plotted as individual ticks or marks along the *y*-axis, corresponding to the neuron identity or trial number (row). The *x*-axis represents time relative to a specific event or trial onset. This could be aligned to a stimulus, behavioural event or another temporal reference point. Patterns such as synchronized firing or response variability can be observed.

Building on the concept of spike raster plots, the peri-stimulus time histogram (PSTH) is a common analysis approach applied to MEA recordings to determine the relationship between an external stimulus (such as an air puff) and how the recorded neurons respond (Fig. 4h). The PSTH is constructed by generating a histogram of the average spike count of recorded neurons within small time bins (~1–5 ms consecutive time windows) preceding and following the stimulus and time locked to the stimulus across all trials of a particular type and across all neurons or a particular neuron class. The histogram gives the average temporal response of a class of neurons to a particular event. Often, the histogram is smoothed using a Gaussian or moving average[145,155].

**Correlation and dimensionality reduction approaches.** With the increasing channel count of MEAs and the increasing complexity of experiments comes increasing complexity in the data. Applying dimensionality reduction approaches to sorted spike data from many simultaneously recorded neurons has become a useful approach for uncovering underlying network function[156,157]. These approaches include state space and population vector approaches, as well as advanced modelling of the neural processes from the data. For a review, see ref. 158.

## Applications

The use of in vivo MEAs has had a great impact on our understanding of the role of neuron firing in brain function, particularly with respect to groups of neurons and how they interact at the circuit and network level and across brain regions. In this section, we highlight some of the key applications for in vivo MEAs, providing a brief overview of some of the types of experiments that can be pursued using in vivo MEAs.

### Sensory, cognitive and motor functions

Simultaneous MEA recordings of populations of single neurons allow the study of single neuron resolution network dynamics within and between brain regions, which give rise to sensory processing, decision-making and sensory–motor transformations. Using chronic implants for this purpose also allows the study of the neural underpinnings of behavioural learning[159].

MEAs have been widely used in basic neuroscience research on the neural basis of motor and sensory functions in all sensory domains[160–165]. Our knowledge of the basic science behind these functions has greatly informed the clinical use of MEAs, including the design of decoding algorithms and the choice of stimulation regimes for bidirectional BCI[166].

**Brain–machine interfaces.** BCIs[6] are electronic systems that provide direct communication between the brain and an external computer or device, bypassing neural systems impaired by injury or disease[7]. Understanding and improving BCIs has grown into a large research area owing to the initial success of BCIs in non-human primates and then in human clinical trials. Successful demonstrations of BCIs have been made using intracortical MEAs to help restore, to a certain extent, lost motor and sensory capabilities. The initial successful applications of BCI would not have been possible without the MEA technology described here as the resolution of neural recordings made by other means is not sufficient for their use as a control signal.

The basic neurophysiology underlying BCIs is that the firing rate of many motor neurons is closely related to the kinematics (for example, the velocity) of both executed and imagined movements[167,168]. Therefore, firing rates of a group of neurons can be used to continuously infer intended movement velocity of a limb through statistical decoding algorithms[169–172]. Integration of the decoded velocity over time can be used to compute displacement and therefore limb location. When these neural signals are used to provide control signals to a robotic manipulator with multiple degrees of freedom, reach-to-grasp movements including opening and closing a robotic gripper can be made using a BCI-controlled robotic limb[173,174].

Bidirectional BCIs, which apply electrical stimulation and record neural activity, have been used to provide tactile feedback for hand–object interactions. Tactile sensations can be artificially elicited through intracortical microstimulation in the somatosensory cortex[14,175]. This approach has been used to enable a person with paralysis to substantially improve reach-and-grasp performance using a robotic limb. Similar principles apply to eliciting percepts in other sensory domains[176].

### Learning, memory and reward

MEAs have been essential to our understanding of the neural basis of learning and memory in the complex hippocampal–entorhinal system. Our understanding of the dynamic interplay between place cells[177] and grid cells[178] that control spatial orientation and place memory, as well as hippocampal theta rhythms and replay and how these impact learning, memory and behaviour, would not have been possible without MEAs capable of obtaining stable single-unit recordings from many simultaneously recorded units in freely moving animals performing complex behavioural experiments[179]. Hippocampal electrophysiology to understand the neural basis of learning and memory remains a highly active area of research, which relies heavily on advances in MEA technology, and continues to advance our fundamental understanding of these essential neural processes.

### Peripheral nerves

MEAs have been used in peripheral nerves to monitor, disrupt or replace sensory signals and activate muscles and organs[180,181]. In the periphery, investigation of skin sensor signals or motor fibre activation requires SUA or at least MUA resolution; however, mass activity in compound nerve action potentials can be used for simple control tasks such as cursor control. Both sensory[182,183] and motor signals[184] can be used for bidirectional neural prosthesis control. For prosthesis control in both unidirectional and bidirectional settings, sliding averaging and binning are used to smooth the signal and assign an action when a threshold is reached. Conduction velocity can be measured if signals are recorded from fibres of a single diameter[185–187].

Most developments in peripheral MEAs have been driven by translational objectives, such as restoring movement after spinal cord injury by delivering sensory feedback through nerve stimulation and the motor control of prosthetic limbs[188–190]. Stimulation of nerves after amputation using true MEAs to deliver sensory feedback for grasp and gait[191–195] has been successfully translated into human clinical studies. Non-penetrating peripheral arrays[107,196], although not comprising microelectrodes in the strictest sense as their electrodes have a larger geometric surface area than intracortical MEAs, operate on similar principles and have been tested in clinical trials to restore bladder voiding[197,198], grasp[199], gait[200] and drop foot[201–203] and to record grasp force[204–207] in clinical trials in persons with paralysis.

There is still much work to be done optimizing MEA interfaces for the individuals who can benefit from them[208]. Needle electrodes are a standard tool in acute microneurography for neurological diagnostics[209]; however, micromachined electrode arrays have not yet been used for acute neuronal diagnosis in humans, except in the case of flexible arrays for intramuscular electromyographic recordings[210]. Comprehensive anatomical studies[211] have shown that sieve electrodes[107] used for regeneration allow nerve fibres to grow through them; however, the distribution of fibre diameter, type and sensory and motor functions are no longer preserved as in the intact nerve. Therefore, no first in-human translational studies have been conducted as of the publication of this article.

## Reproducibility and data deposition

### Obtaining quality data

Selecting recording amplifiers with a high input impedance is key for high-quality recordings. A good recording amplifier for electroencephalography will not necessarily be suitable for MEA recordings. Noise in electrical engineering might comprise thermal and flicker noise, whereas the same term in neuroscience might reflect the undesired background activity of the brain. Therefore, parameters and equations might be different and translation might be necessary to come to a useful comparison. Understanding these differences is important to compare and select MEAs, amplifiers and filters.

Before implantation, electrochemical impedance spectroscopy should be used or impedance should be measured at 1 kHz

(Supplementary Note 3) to ensure that electrodes are functional and within the expected range for their type. For chronic experiments, impedance can be measured before recording sessions to assess how electrode performance might have changed over time, as these can affect signal quality[104,212,213].

To record high-quality SUA, the soma-to-electrode distance should typically be in the range of <100 µm (refs. 214,215) and therefore care should be taken when placing electrodes to ensure that correct regions are targeted and good contact is made between electrodes and tissue.

The single-unit yield, the number of single units per electrode site, SNR and single-unit amplitude can be used as metrics to assess recording quality for both acute and chronic experiments[216]. Single-unit inclusion criteria must be held constant for comparisons between experimental conditions to be meaningful[217]. For chronic experiments, tracking the same neurons over many days and being able to confidently assign the spikes recorded over multiple sessions as belonging to the same unit can be extremely valuable. Metrics such as auto-correlograms, pairwise cross-correlograms, waveform shape, ISI distribution, mean firing rate and stimulus selectivity can collectively be used as a basis for determining neuron identity in recordings across days[49,61,218,219].

### Reporting standards

In general, as much detail as possible should be reported to aid in reproducibility efforts. Information on the experimental subjects should be reported, including animal number, strain, age, sex, implantation surgery, surgical or pharmacological intervention (if any) and behavioural paradigm[220]. Details on the MEA design should include its dimensions; electrode size, material, number and spacing; and details on the amplifier and recording equipment and instrument settings used to collect the data. Analysis steps should also be reported, with information regarding the spike sorting pipeline used and how any post sorting analysis was conducted. Custom scripts should be described if used and made publicly available.

**Reproducibility and reporting of spike sorting parameters.** Each sorting algorithm uses spike features differently and therefore performance is dependent on the nature of the data set (such as array type, cell type and experimental conditions). In a community-driven effort to benchmark the performance of sorting algorithms using synthetic and observational data sets, no single algorithm emerged as the best performer when examined across all data sets[221]. Developing a sorting algorithm that performs well under all conditions remains difficult because of the absence of 'ground truth' data sets of adequate size. To identify the algorithm with the best sorting performance for a specific data set, several algorithms should be tested and examined against manually curated data (and ground truth data if available). Although outputs from different sorters do not directly validate the results, reporting results from multiple sorters helps improve the transparency, accessibility and reproducibility of future neuroscience research.

Regarding spike sorting data quality metrics, the field is moving towards generating common reporting standards but currently lacks a consensus. The Allen Institute and International Brain Laboratory have recently introduced standards and benchmarks for SUA reporting, including the percentage of ISI violations (<0.5%), presence ratio (>0.9), spike amplitude cut-off (<10% estimated spikes below the low amplitude cut-off) and firing rate (>0.1 Hz and <500 spikes per second)[81,222]. However, the nature of the data will always result in a range of reliable assignments and it is critical that the stringency of inclusion criteria matches the scientific questions being addressed. For example, if a small number of errors in spike sorting will undermine a result (for example, in spike timing-based analysis), then stricter inclusion criteria might be necessary. Greater adoption of reporting quality metrics, commonly available as outputs from sorting algorithms, would strengthen reproducibility efforts.

### Data sharing

The public availability of neuroscience data has increased markedly in recent years through efforts such as the International Brain Laboratory, Allen Institute, Dandi, Zenodo, Figshare and Globus. Despite this positive trend, widespread data sharing faces many challenges. First, neuroscience data are diverse. Metadata are needed about the experimental subjects (species, genotype, age and weight), type of recording (LFPs, MUA and SUA), MEAs (number of channels, shanks and selected channels), brain region(s), experimental conditions (stimuli, trial structure and recording environment), sensors to measure bodily signals (temperature and blood pressure) and description of behaviour (performance, motion tracking, acceleration and other video data). Moreover, data and metadata types and formats are constantly changing as scientists develop new tools for recording and transforming data[223–225] and tracking behaviour[122,226]. Second, individual researchers develop their own methods for storing and processing data, which work in the conditions under which they were created but might not be portable. Without field standards, data might be largely inaccessible to others even if they are made available, making it difficult to share across laboratories. One of the main goals of Neurodata Without Borders[227] is to provide a framework for documenting data so that other researchers can understand and further analyse it. Making neuroscience data findable, accessible, interoperable and reusable[228] requires community consensus and collaboration between researchers and programmers. The third challenge is developing and maintaining the IT infrastructure for shared data, including repositories and search engines, as these are associated with considerable costs.

## Limitations and optimizations

In vivo MEAs have had a great impact on our understanding of the nervous system and they remain an unparallelled tool for recording electrical signals from many neurons at high spatiotemporal resolution in anaesthetized and behaving animals. Nevertheless, there are limitations to the technology which will be discussed here, as well as ways researchers are working to overcome the current limits of the technology.

### Denoising

Electrophysiological signals are small and so environmental electrical noise must be carefully managed. All electrophysiology systems require denoising. The most broadly useful consideration is the system ground. Every part of the system should share a common ground, from array to computer. The subject animal itself can be a source of electrical noise, acting like an antenna for electromagnetic interference, and experiments should therefore be performed in a Faraday cage to reduce this effect. System noise should be measured before an experiment, which can be achieved by submerging the electrodes in an electrolyte solution and feeding a sine or square wave of ~1 kHz and 0.5–1 mV into the buffer using a platinum wire; a noise level above 10 µV indicates that further measures must be taken to reduce system noise.

Troubleshooting noise starts with observing the raw, unfiltered data. If noise appears on a single channel or on all channels located on

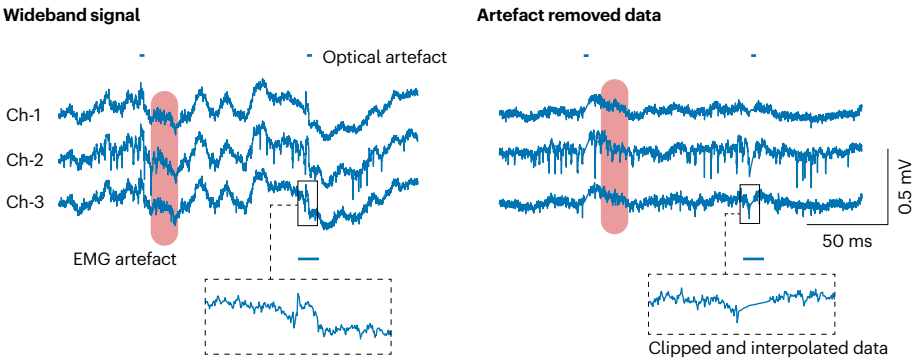


**Fig. 5 | Artefact removal.** Example multichannel recording traces before (wideband signal) and after (artefact removed data) artefact removal, using common-average referencing to remove muscle artefacts (electromyography (EMG) artefact) and stimulus-locked clipping and interpolation to remove optical artefacts.

a shank, then the channel or shank is likely broken. Wideband noise across all channels might indicate a broken ground or reference connection, headstage or cable. Replacing the cable or headstage can resolve the issue. Testing for a broken ground/reference in a chronic implant typically requires anaesthetizing the animal and testing the continuity of the ground, which can be challenging without damaging the implant. Electromagnetic noise is likely caused by power cables in close proximity to the rig and appears as 50 or 60 Hz noise across all channels. Moving the rig away from electrical outlets or placing a ground plane below the rig can mitigate line noise. For a flowchart of noise troubleshooting, see Supplementary Fig. 1.

## Artefact removal

Recording from head-fixed, awake or freely moving rodents can introduce highly synchronous artefacts caused by volume-conducted muscle activity (Fig. 5). Consummatory behaviour (chewing or drinking) will also cause artefacts. Performing median subtraction is a common technique used to achieve a stable baseline and reduce motion artefacts.

Recording is frequently combined with either electrical or optogenetic stimulation and both can create stimulation artefacts in recordings. Optogenetic stimulation will trigger light-induced artefacts owing to the photoelectric effect, which are not consistent across channels, more pronounced at onset and offset and can take the form of a spikelet[229,230]. To prevent such artefacts from propagating to spike sorting, raw data should be clipped out in the interval shortly before (0.15 ms) and after (0.8 ms) each brief (<3 ms) stimulus pulse. If longer-duration optical pulses are used (>3 ms), each onset and offset artefact should be removed to improve the quality of spike sorting (Fig. 5). This approach, as well as regression-based methods, can be used for electrically induced stimulation artefacts[231]. For electrical stimulation, care should be taken not to saturate the amplifier on recording electrodes (stimulating and adjacent electrodes might not be recordable) to maximize the success of artefact removal[232].

## Biocompatibility

Array implantation triggers a non-specific FBR[233–235], which impedes the ability of the array to record neuronal signals over time. Although hundreds of units can be recorded for weeks, many groups have reported that the number of single units decreases over time[236,237], with some finding only ~50% of initially recorded neurons were recorded 1 week after implantation[238]. MEAs must be designed to minimize undesired tissue reactions and maintain the functionality of the device.

Material and device design, as well as surgical procedures and insertion techniques, contribute to overall biocompatibility[239,240] (Fig. 6). Materials must be non-toxic and should not induce local or systemic cell proliferation, allergic, pyrogenic or anaphylactic reactions (Fig. 6f). Degradation or corrosion products should not be released (Fig. 6c). Useful recommendations can be found in the international standard 'Biological Evaluation of Medical Devices' (ISO 10993). Residues from fabrication and post-processes should be considered and cleaning should be performed to remove residues before sterilization. Surface treatments can also be used to modify the surface energy and thereby protein adsorption and cell attachment[241,242].

The weight, size and stiffness (Young's modulus) of an MEA contribute to the moment of inertia with which forces interact between implant and tissue[243] (Fig. 6d), and flexible electrodes have been introduced to minimize tissue reactions (Fig. 6e) and improve long-term performance[58,61,244]. Tethering forces between the array and external hardware, as well as micromotion from blood flow and breathing, also contribute to the FBR (Fig. 6e). The voltage-based release of drugs such as dexamethasone from stimulated electrodes coated with conjugated polymers has been explored for reducing the FBR[245–250] (Fig. 6b). Furthermore, the use of the neural adhesion protein L1 as a bioactive coating to promote stable neural integration with MEAs has shown promise for improving tissue integration and long-term device performance[246,251–254].

MEAs explanted after chronic use are not commonly examined; however, these studies can be illuminating as several have identified signs of MEA degradation and of FBR in the surrounding neural tissue. Analysis of explanted Utah arrays[236,255], cochlear implants[256] and peripheral MEAs[257,258] has shown substantial corrosion of electrodes and signs of gliosis and calcification in the tissue surrounding the implant[259]. In one study using flexible arrays, implanted rats showed increased gene expression associated with wound healing and angiogenesis and the upregulation of a subset of immediate early genes compared with the pre-injury state after 18 weeks of implantation, indicating ongoing structural and functional remodelling of the neural tissue around the implant[260]. Further investigation is necessary to better understand the long-term biological effects of array implantation, which will be valuable in informing future use of MEAs in humans.

## Device stability and longevity

Longevity in the context of MEAs refers to the functional lifespan of the electrodes within the biological environment. Typical device failures are due to delamination from and between passivation layers[261] for both rigid and flexible arrays. When insulation materials are deposited directly on noble metals, they do not form chemical bonds, allowing for liquid ingress after implantation. The addition of a silicon carbide interlayer improves adhesion, extending the device lifetime[181,257,262].

MEAs can be made entirely from SiC, although this makes them rigid, similar to silicon arrays[263,264]. Another method to improve the longevity of MEAs is to deposit a thin oxide layer between polymer layers[265] to create a quasi-hermetic enclosure to protect the backend components, which could also be extended to the entire MEA[266] and has been shown to increase longevity in accelerated ageing tests for flexible MEAs[267].

**Longevity of stimulation electrodes.** Requirements for stimulation electrodes are more stringent than for recording-only sites. Stimulation electrodes must withstand much higher potentials, especially in chronic applications in which the formation of a glial scar leads to a progressive increase in the polarization potential necessary to achieve the same level of injected current. This problem can be overcome by using electrode materials with a higher charge injection limit and by improving the tissue–electrode interface to reduce the FBR[268] (Fig. 6). One promising approach to reducing the FBR and thereby the chronic stimulation threshold is using ultra-flexible arrays that form scar-free integration with the host tissue. In one study using ultra-flexible MEAs in mice, stable stimulation thresholds were demonstrated for over a year with extremely low detection thresholds[269,270], although these data must be considered cautiously when extending to large animal models and humans. Although beneficial in reducing FBR, ultra-flexible arrays might have reduced robustness and durability. There is therefore a balance between designs that are sufficiently small and flexible to minimize biological interference[271] and also sufficiently robust to remain functional over the lifespan of the experiment. For additional details on stability assessment, see Supplementary Note 4.

## Surgical challenges

MEAs are typically inserted using a micromanipulator while monitoring for buckling. The dura mater provides the primary resistance to device insertion (Young's modulus of ~50 MPa)[272] compared with the parenchyma, which has a Young's modulus of only ~5 kPa. Typical MEAs cannot penetrate the dura mater, except for in mice as they have a thin dura. In most subjects, the dura should be removed before array insertion. However, without proper training, dura removal can damage the parenchyma, leading to bleeding, brain swelling and dehydration[273], which in turn reduces single-unit yield and data quality. Insertion of flexible probes often requires the aid of a transient shuttle enclosure or coupling with a stiff shuttle; for stiff probes or flexible probes inserted with the aid of a stiff shuttle, sharpening the array or shuttle tip can allow insertion without removing the dura[274].

Less total force is required to insert a single-shank device than a multi-shank one and, when combined with the smaller footprint of single-shank devices, can result in less tissue damage resulting from them. Very slow insertion speed (<1 µm $s^{-1}$) can further minimize tissue damage, resulting in higher unit yield[91,275]. Using a micromanipulator equipped with a micron-scale ultrasonic vibration generator (such as NeuralGlider) for MEA insertion can reduce dimpling and tissue displacement[276]. A slight overshoot and then retraction are also effective at reducing cortical dimpling[277]. For Utah MEAs, the preferred insertion method is high-speed insertion (>8.3 m $s^{-1}$) using a pneumatic inserter[278,279]. Custom 3D-printed holders, using surgery planning software[280] and performing practice surgeries can also improve the surgical approach.

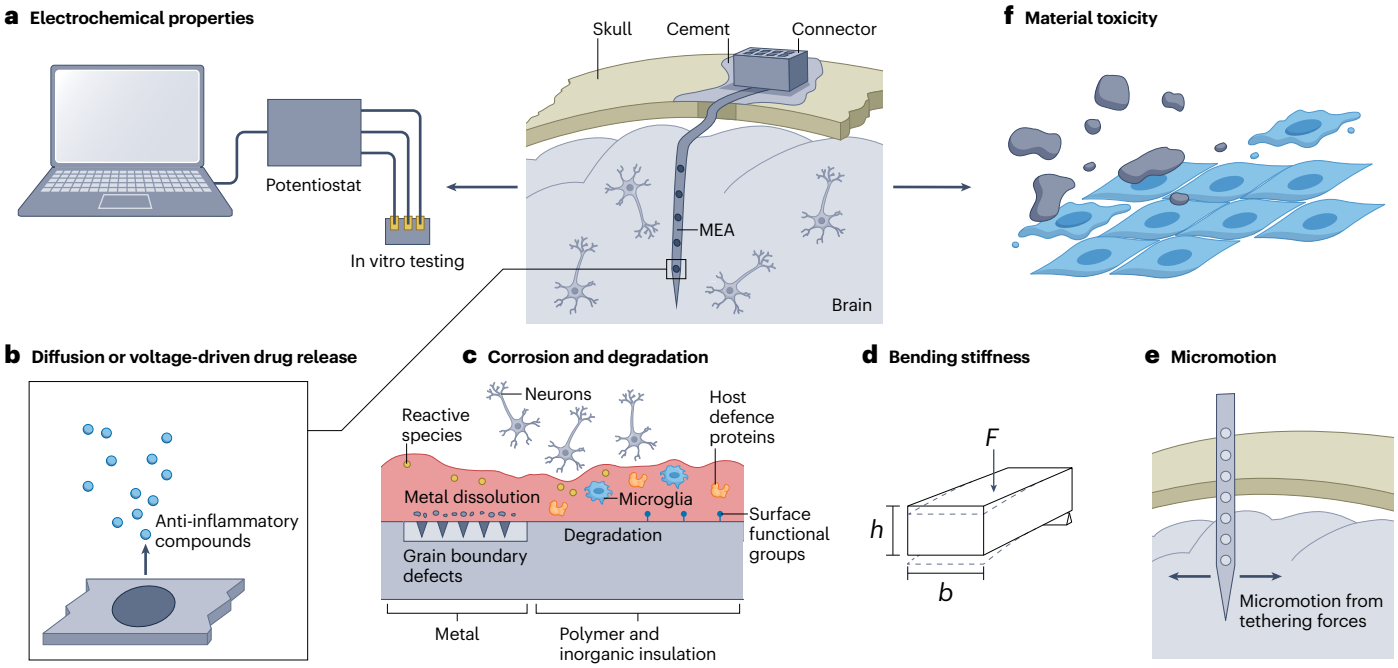


**Fig. 6 | Factors governing biocompatibility and foreign body response.** A flexible microelectrode array (MEA) implanted in the cortex, with a connector cemented to the skull. **a**, Electrochemical characterization can determine the stimulation threshold that will not degrade the MEA. **b**, Anti-inflammatory therapies can be built into the device and released to reduce the foreign body response (FBR). **c**, Material and biological factors leading to degradation include but are not limited to metal dissolution and reactions to insulation leading to inflammation and the production of reactive oxygen species, which can in turn damage the device. The host response can lead to gradual encapsulation of the device by microglia and proteins. **d**, Mechanical properties governing array insertion such as bending stiffness (*F*, force; *h*, height; *b*, base) impact the FBR. **e**, Tethering forces and micromotion induce FBR. **f**, Dissolution of potentially toxic by-products of the MEA or over-stimulation can induce FBR.

## Glossary

**Active electronics**
Electrical circuit components such as transistors that can amplify or control the flow of electricity and require an external power source.

**Application-specific integrated circuit**
Application-specific integrated circuit (ASIC) is an integrated circuit that is designed for a specific use and is not reprogrammable once it is fabricated.

**Closed-loop experiment**
An experiment involving a closed-loop system uses feedback control where a portion of the output signal is fed back into the input.

**Cocktail party problem**
The problem of perceiving and isolating speech in a noisy setting in which audio signals overlap in both frequency and time.

**Common average referencing**
A technique used to improve the signal-to-noise ratio in electrophysiological recordings; it involves calculating the average potential across all electrodes or channels and using this average as a reference point for each individual electrode or channel.

**Device lifetime**
Device lifetime is the period of time that a device can be used safely and effectively.

**Direct current offsets**
Also known as DC offset or DC bias; the steady-state voltage on the electrode when no signal is applied.

**Fascicles**
Small bundles of nerve fibres that are enclosed within a connective tissue sheath. They are structural units of nerves, providing support and protection to the nerve fibres within.

**Foreign body response**
(FBR). An inflammatory process that is triggered when a foreign body (for example, a microelectrode array) is implanted into the body.

**Grid cells**
Neurons in the entorhinal cortex that fire in a hexagonal grid-like pattern as an animal moves through space, providing a coordinate system for spatial navigation and positioning.

**Headstage**
A set of electronics mounted on the head of an animal to convey signals to and from microelectrode arrays.

**Hippocampal theta rhythms**
A type of local field potential oscillation in the 4–12 Hz range observed in the hippocampus, associated with navigation, learning and memory processing.

**Listening volume**
The volume of tissue from which an electrode can pick up the electrical signal.

**Membrane potential**
The voltage difference across the plasma membrane of a cell, created by the unequal distribution of ions (for example, sodium, potassium and chloride) inside and outside the cell. The membrane potential is essential for the conduction of electrical impulses and the generation of action potentials.

**Microdrive**
A device that holds a microelectrode array (MEA) and can be mounted on an animal head. Microdrives are usually used to insert MEAs into the brain slowly and precisely and for convenient recovery of MEAs at the end of experimentation.

**Neuronal ensembles**
A population of neurons involved in a specific neural circuit or computation.

**Passive MEAs**
Electronic components that transmit electrical energy but do not generate it and do not require an external power source to function.

**Place cells**
Neurons in the hippocampus that become active when an animal is in a specific location in its environment. They help form cognitive maps for spatial navigation and memory.

**Single-unit activity**
(SUA). Refers to the recording of electrical activity from a well-isolated single neuron, typically recorded from a microelectrode on a microelectrode array. It captures its action potentials (spikes) over time with high temporal and spatial resolution.

**Spike trains**
A sequence of recorded action potentials or spikes.

**System ground**
A common return path for electrical currents in the system. It is usually grounded to Earth, meaning it has a direct electrical connection to the Earth.

**Tuning functions**
Firing rate as a function of an external variable or variable(s) often across a continuum of stimulus values.

### Data challenges

High-density MEAs generally generate 80–185 gigabytes per hour of raw data[44,48,88]. Long-term experiments can generate prohibitively large data sets even when recording from MEAs with fewer sites. Data management infrastructure should be in place before data collection begins to prevent bottlenecks. Oversampling (for example, digitizing raw traces at >30 kHz) should be avoided, as it only results in larger data files without providing additional information. Sampling rates between 12.5 kHz and 30 kHz are optimal[281]. Given the high cost associated with large data volumes, new strategies are needed to compress neuroscience data[282].

### Cable management

Given that most neurophysiology experiments require multiple instruments that all must communicate with each other via wired connections, routing cables between subjects and equipment can become a challenge, especially for behavioural experiments. Cables should be secured to prevent accidental detachment and interruption of data collection, especially for those connected to movable apparatus or attached to or within the reach of subjects. Any restriction of a subject's behaviour owing to the presence of cables should be minimized. In freely moving paradigms, a swivel or helium balloon[283,284] can be used to support the weight of cables and keep them above the arena so as not to interfere with behaviour. A commutator can reduce tangling of suspended cables as subjects rotate, if needed. Cable movement should also be restricted to minimize capacitive coupling artefacts in the recording. Besides choosing cables of small size, wireless systems can be adopted when applicable.

### Wireless recording

Untethered recording of animals larger than mice can use a data logger for gathering data; this set-up involves storing data locally on an SD card that is synchronized with environmental cues wirelessly. The duration of the experiment is limited by the capacity of the battery, which is determined by the size and weight of the headstage that the animal can carry. This approach is particularly useful for studying social interactions

and natural behaviour in large groups of animals[285–287]. In rodents, wireless recording and electrical and optogenetic stimulation can be performed. Power and range constraints limit the versatility of this approach; however, work is underway to improve this functionality[287–290]. Wireless recordings using high-channel-count arrays remain challenging[291] and few systems are commercially available for this purpose, although data loggers are available from SpikeGadgets for use with Neuropixels. Bandwidth constraints are a major bottleneck for wireless transmission. Battery efficiency is also one of the limiting factors as transmitters with an effective range have high power demands. Bluetooth is the most cost-effective and battery-efficient transmission standard, but the bandwidth is still limiting and efficient data compression requires some loss in data fidelity.

## Outlook

The use of in vivo MEAs is likely to increase in the future as technological developments continue to advance, making current devices more accessible and creating MEAs that can address an even broader range of scientific questions. Some of the new developments underway are described here.

### New electrode technologies

Electrical recording and stimulation are the most common modalities used with MEAs; however, additional modalities can be integrated such as optical stimulation and imaging, electrochemical sensing and drug delivery[292,293]. Miniature sensor components for pH, temperature and mechanical strain can also be incorporated into MEAs to further expand functionality[294–299].

Flexible MEAs offer new opportunities for combining electrophysiological recordings with other experimental modalities. Unlike rigid electrodes, the backend connectors can be positioned away from the implantation site to reduce the probe shadow for large-area two-photon microscopy or speckle imaging[271,300]. It is also possible to make partially or fully transparent flexible MEAs for combination with imaging and optogenetics[301–305] and to remove the photoelectric artefact on the traces, provided that the amplifier is not saturated[302]. Flexible MEAs also show great promise for use in the spinal cord[306–308]. For clinical and preclinical applications, X-ray markers can be added for fluoroscopically guided insertion[309]. Following recent trends in the optimization of fabrication methods for thin flexible arrays, their electrode density and channel count should soon approach that of high-density rigid arrays[306].

MEAs can be used as electrochemical sensors to detect electroactive neurochemicals as redox peaks using fast scan cyclic voltammetry[310]. Surface modification strategies and electrochemical techniques have been used to detect many different neurochemicals of interest. Non-electroactive neurochemicals can also be detected using enzymes that produce a secondary analyte (often hydrogen peroxide) that is readily detected[311,312] or aptamers that are selected to have specific affinity to neurochemical targets[313–315].

Using transistors as electroactive sites for recording neural activity is a promising approach as it enables local amplification for high SNR[316]. In addition, they are also capable of electrochemical sensing[315,317,318]. Both inorganic and organic transistors can be used, with organic transistors being more compliant and suitable for constructing flexible MEAs[319,320].

Optical signal transmission technologies, such as wavelength division multiplexing using electrical-to-optical couplers integrated on recording sites or pre-amplifiers, could allow signals from different electrodes to be converted to light of different wavelengths and sent through optical fibres simultaneously, allowing switchless high-channel-count recording[321].

Delivering drugs using MEAs is a way to directly modify the cellular environment locally around the MEA, with a wide range of potential applications. Surface-bound nanocarriers or porous nanoparticles integrated into the electrode coating can be used for spatially and temporally controlled drug delivery[292,322–325]. Systemically delivered nanocarriers responsive to remote release triggers such as magnetic, ultrasound or infrared signals can supplement local delivery for modulation at multiple spatial scales[326–328].

Advances in fabrication techniques[329] have expanded the applications of in vivo MEAs. The manufacturing of smaller, more flexible designs with greater shape customizability has expanded the range of model organisms for which suitable MEAs are available and MEAs have now been designed for use in *Caenorhabditis elegans*[330], insects[331], fish[332] and sea slugs[308,333]. Furthermore, new flexible and multimodal MEAs[334,335] have been used in the enteric nervous system of the gastrointestinal tract[336], an organ system that would greatly benefit from high-density electrophysiological mapping and stimulation studies.

### Leveraging machine learning

Advanced machine learning has been adopted in behavioural neuroscience for automatic image analysis, as this is a more general application of the technology commonly implemented across disciplines[122,337]. More restricted machine-learning approaches have been used on large electrophysiology data sets to extract latent features. To date, these models have been limited and require human curation and optimization of the model for the data set. Machine learning is poised to make a larger impact on the field as it is being explored for the automation of spike sorting[338] and the analysis of large data sets with the ability for self-optimization and automatic feature extraction. Machine learning could also be applied for the design and implementation of closed-loop experiments for real-time classification and tailoring of stimuli based on current brain state, with applications for advanced BCIs[207,339].

### Applications for bioelectronic medicine

Recent studies on cortical electrical neuromodulation for learning and memory have shown promise for neuroprosthetic systems treating cognitive disorders (reviewed elsewhere[340,341]). Autonomic nerves are promising targets for PNS interfaces. The vagus nerve and its branches, as well as other autonomic nerves, can be stimulated to treat hypertension, chronic obstructive pulmonary disease, obesity, depression, chronic pain, rheumatic arthritis and autoimmune diseases[342–344]; however, many fundamental research questions need to be addressed to understand the underlying processes and neural semiotics involved[345,346].

### Conclusion

The future of in vivo MEAs in neuroscience is promising with ongoing advancements and innovations. These technological advancements, driven by a synergy among basic neuroscience, material science and micro-technological and nano-technological engineering, hold great promise for advancing our understanding of neural circuits and behaviours as well as paving the way for innovative applications in neuroprosthetics and bioelectronic medicine.

Published online: 08 May 2025

## References


1. Cogan, S. F. Neural stimulation and recording electrodes. *Annu. Rev. Biomed. Eng.* **10**, 275–309 (2008).
2. Dunlop, J., Bowlby, M., Peri, R., Vasilyev, D. & Arias, R. High-throughput electrophysiology: an emerging paradigm for ion-channel screening and physiology. *Nat. Rev. Drug Discov.* **7**, 358–368 (2008).
3. Passaro, A. P. & Stice, S. L. Electrophysiological analysis of brain organoids: current approaches and advancements. *Front. Neurosci.* **14**, 622137 (2021).
4. Johnstone, A. F. M. et al. Microelectrode arrays: a physiologically based neurotoxicity testing platform for the 21st century. *NeuroToxicology* **31**, 331–350 (2010).
5. Donoghue, J. P. Connecting cortex to machines: recent advances in brain interfaces. *Nat. Neurosci.* **5**, 1085–1088 (2002).
6. Hofmann, U. G. & Stieglitz, T. Why some BCI should still be called BMI. *Nat. Commun.* **15**, 6207 (2024).
7. Fraser, G. W., Chase, S. M., Whitford, A. & Schwartz, A. B. Control of a brain–computer interface without spike sorting. *J. Neural Eng.* **6**, 055004 (2009).
8. Santhanam, G., Ryu, S. I., Yu, B. M., Afshar, A. & Shenoy, K. V. A high-performance brain–computer interface. *Nature* **442**, 195–198 (2006).
9. Hochberg, L. R. et al. Neuronal ensemble control of prosthetic devices by a human with tetraplegia. *Nature* **442**, 164–171 (2006).
10. Collinger, J. L. et al. High-performance neuroprosthetic control by an individual with tetraplegia. *Lancet* **381**, 557–564 (2013).
11. Soekadar, S. R., Birbaumer, N. & Cohen, L. G. in *Systems Neuroscience and Rehabilitation* (eds Kansaku, K. & Cohen, L. G.) 3–18 (Springer, 2011).
12. Brumberg, J. S. et al. Brain–computer interfaces for speech communication. *Speech Commun.* **52**, 367–379 (2010).
13. Gonzalez-Lopez, J. A., Gomez-Alanis, A., Martín Doñas, J. M., Pérez-Córdoba, J. L. & Gomez, A. M. Silent speech interfaces for speech restoration: a review. *IEEE Access* **8**, 177995–178021 (2020).
14. Flesher, S. N. et al. A brain–computer interface that evokes tactile sensations improves robotic arm control. *Science* **372**, 831–836 (2021).
15. Zeng, F.-G., Rebscher, S., Harrison, W., Sun, X. & Feng, H. Cochlear implants: system design, integration, and evaluation. *IEEE Rev. Biomed. Eng.* **1**, 115–142 (2008).
16. Lewis, P. M., Ackland, H. M., Lowery, A. J. & Rosenfeld, J. V. Restoration of vision in blind individuals using bionic devices: a review with a focus on cortical visual prostheses. *Brain Res.* **1595**, 51–73 (2015).
17. Chen, Z. et al. Soft, bioresorbable, transparent microelectrode arrays for multimodal spatiotemporal mapping and modulation of cardiac physiology. *Sci. Adv.* **9**, eadi0757 (2023).
18. Choi, J. S., Lee, H. J., Rajaraman, S. & Kim, D.-H. Recent advances in three-dimensional microelectrode array technologies for in vitro and in vivo cardiac and neuronal interfaces. *Biosens. Bioelectron.* **171**, 112687 (2021).
19. Choi, J. S. et al. Nanopatterned Nafion microelectrode arrays for in vitro cardiac electrophysiology. *Adv. Funct. Mater.* **30**, 1910660 (2020).
20. McAvoy, M. et al. Flexible multielectrode array for skeletal muscle conditioning, acetylcholine receptor stabilization and epimysial recording after critical peripheral nerve injury. *Theranostics* **9**, 7099–7107 (2019).
21. Liu, J. Y. H., Du, P., Chan, W. Y. & Rudd, J. A. Use of a microelectrode array to record extracellular pacemaker potentials from the gastrointestinal tracts of the ICR mouse and house musk shrew (*Suncus murinus*). *Cell Calcium* **80**, 175–188 (2019).
22. Leal, J., Shaner, S., Jedrusik, N., Savelyeva, A. & Asplund, M. Electrotaxis evokes directional separation of co-cultured keratinocytes and fibroblasts. *Sci. Rep.* **13**, 11444 (2023).
23. Cerina, M., Piastra, M. C. & Frega, M. The potential of in vitro neuronal networks cultured on micro electrode arrays for biomedical research. *Prog. Biomed. Eng.* **5**, 032002 (2023).
24. Obien, M. E. J., Deligkaris, K., Bullmann, T., Bakkum, D. J. & Frey, U. Revealing neuronal function through microelectrode array recordings. *Front. Neurosci.* **8**, 423 (2015).
25. Chandrasekaran, S. et al. Historical perspectives, challenges, and future directions of implantable brain–computer interfaces for sensorimotor applications. *Bioelectron. Med.* **7**, 14 (2021).
26. Shokoueinejad, M. Progress in the field of micro-electrocorticography. *Micromachines* **10**, 62 (2019).
27. Schalk, G. & Leuthardt, E. C. Brain–computer interfaces using electrocorticographic signals. *IEEE Rev. Biomed. Eng.* **4**, 140–154 (2011).
28. Krass, J. K. et al. Technology of deep brain stimulation: current status and future directions. *Nat. Rev. Neurol.* **17**, 75–87 (2021).
29. Grienberger, C., Giovannucci, A., Zeiger, W. & Portera-Cailliau, C. Two-photon calcium imaging of neuronal activity. *Nat. Rev. Methods Primers* **2**, 1–23 (2022).
30. Qiang, Y. et al. Crosstalk in polymer microelectrode arrays. *Nano Res.* **14**, 3240–3247 (2021).
31. Stieglitz, T. & Gross, M. Flexible BIOMEMS with electrode arrangements on front and back side as key component in neural prostheses and biohybrid systems. *Sens. Actuators B Chem.* **83**, 8–14 (2002).
32. Gablech, I. & Głowacki, E. D. State-of-the-art electronic materials for thin films in bioelectronics. *Adv. Electron. Mater.* **9**, 2300258 (2023).
33. Yi, D., Yao, Y., Wang, Y. & Chen, L. Design, fabrication, and implantation of invasive microelectrode arrays as in vivo brain–machine interfaces: a comprehensive review. *J. Manuf. Process.* **126**, 185–207 (2024).
34. Lopez, C. M. et al. An implantable 455-active-electrode 52-channel CMOS neural probe. *IEEE J. Solid-State Circuits* **49**, 248–261 (2014).
35. Lopez, C. M. et al. A neural probe with up to 966 electrodes and up to 384 configurable channels in 0.13 µm SOI CMOS. *IEEE Trans. Biomed. Circuits Syst.* **11**, 510–522 (2017).
36. Cui, X., Hetke, J. F., Wiler, J. A., Anderson, D. J. & Martin, D. C. Electrochemical deposition and characterization of conducting polymer polypyrrole/PSS on multichannel neural probes. *Sens. Actuators Phys.* **93**, 8–18 (2001).
37. Bianchi, M. et al. Poly(3,4-ethylenedioxythiophene)-based neural interfaces for recording and stimulation: fundamental aspects and in vivo applications. *Adv. Sci.* **9**, 2104701 (2022).
38. Wise, K. D., Anderson, D. J., Hetke, J. F., Kipke, D. R. & Najafi, K. Wireless implantable microsystems: high-density electronic interfaces to the nervous system. *Proc. IEEE* **92**, 76–97 (2004).
39. Najafi, K., Wise, K. D. & Mochizuki, T. A high-yield IC-compatible multichannel recording array. *IEEE Trans. Electron. Devices* **32**, 1206–1211 (1985).
40. Najafi, K. & Wise, K. D. An implantable multielectrode array with on-chip signal processing. *IEEE J. Solid-State Circuits* **21**, 1035–1044 (1986).
41. Ji, J. & Wise, K. D. An implantable CMOS circuit interface for multiplexed microelectrode recording arrays. *IEEE J. Solid-State Circuits* **27**, 433–443 (1992).
42. Olsson, R. & Wise, K. A three-dimensional neural recording microsystem with implantable data compression circuitry. in *ISSCC. 2005 IEEE International Digest of Technical Papers. Solid-State Circuits Conference* Vol. 1, 558–559 (IEEE, 2005).
43. Dutta, B. et al. The Neuropixels probe: a CMOS based integrated microsystems platform for neuroscience and brain–computer interfaces. In *2019 IEEE International Electron Devices Meeting (IEDM)* 10.1.1–10.1.4 (IEEE, 2019).
44. Angotzi, G. N. et al. SiNAPS: an implantable active pixel sensor CMOS-probe for simultaneous large-scale neural recordings. *Biosens. Bioelectron.* **126**, 355–364 (2019).
45. Ribeiro, J. F. et al. Channels, layout and size scalability of implantable CMOS-based multielectrode array probes. In *2022 International Electron Devices Meeting (IEDM)* 29.6.1–29.6.4 (IEEE, 2022).
46. Seidl, K. et al. CMOS-based high-density silicon microprobe arrays for electronic depth control in intracortical neural recording — characterization and application. *J. Microelectromech. Syst.* **21**, 1426–1435 (2012).
47. Lee, K. H. et al. Electrode pooling can boost the yield of extracellular recordings with switchable silicon probes. *Nat. Commun.* **12**, 5245 (2021).
48. Jun, J. J. et al. Fully integrated silicon probes for high-density recording of neural activity. *Nature* **551**, 232–236 (2017).
49. Steinmetz, N. A. et al. Neuropixels 2.0: a miniaturized high-density probe for stable, long-term brain recordings. *Science* **372**, eabf4588 (2021).
50. Ruther, P., Herwik, S., Kisban, S., Seidl, K. & Paul, O. Recent progress in neural probes using silicon MEMS technology. *IEEE Trans. Electr. Electron. Eng.* **5**, 505–515 (2010).
51. Campbell, P. K., Jones, K. E., Huber, R. J., Horch, K. W. & Normann, R. A. A silicon-based, three-dimensional neural interface: manufacturing processes for an intracortical electrode array. *IEEE Trans. Biomed. Eng.* **38**, 758–768 (1991).
52. Bhandari, R., Negi, S. & Solzbacher, F. Wafer-scale fabrication of penetrating neural microelectrode arrays. *Biomed. Microdevices* **12**, 797–807 (2010).
53. Downey, J. E., Schwed, N., Chase, S. M., Schwartz, A. B. & Collinger, J. L. Intracortical recording stability in human brain–computer interface users. *J. Neural Eng.* **15**, 046016 (2018).
54. Pandarinath, C. et al. High performance communication by people with paralysis using an intracortical brain-computer interface. *eLife* **6**, e18554 (2017).
55. Roh, H. et al. Fabrication of high-density out-of-plane microneedle arrays with various heights and diverse cross-sectional shapes. *Nano-Micro Lett.* **14**, 24 (2021).
56. Zardini, A. S., Rostami, B., Najafi, K., Hetrick, V. L. & Ahmed, O. J. Sea of electrodes array (SEA): extremely dense and high-count silicon-based electrode array technology for high-resolution high-bandwidth interfacing with 3D neural structures. Preprint at *bioRxiv* https://doi.org/10.1101/2021.01.24.427975 (2021).
57. Saleh, M. S. et al. CMU array: a 3D nanoprinted, fully customizable high-density microelectrode array platform. *Sci. Adv.* **8**, eabj4853 (2022).
58. Luan, L. et al. Ultraflexible nanoelectronic probes form reliable, glial scar-free neural integration. *Sci. Adv.* **3**, e1601966 (2017).
59. Wang, X. et al. A parylene neural probe array for multi-region deep brain recordings. *J. Microelectromech. Syst.* **29**, 499–513 (2020).
60. Park, S.-Y. et al. A miniaturized 256-channel neural recording interface with area-efficient hybrid integration of flexible probes and CMOS integrated circuits. *IEEE Trans. Biomed. Eng.* **69**, 334–346 (2022).
61. Zhao, Z. et al. Ultraflexible electrode arrays for months-long high-density electrophysiological mapping of thousands of neurons in rodents. *Nat. Biomed. Eng.* **7**, 520–532 (2023).
62. Brown, M. A. et al. Direct laser writing of 3D electrodes on flexible substrates. *Nat. Commun.* **14**, 3610 (2023).
63. Lee, J. Y. et al. Foldable three dimensional neural electrode arrays for simultaneous brain interfacing of cortical surface and intracortical multilayers. *npj Flex. Electron.* **6**, 1–14 (2022).
64. Abu Shihada, J. et al. Highly customizable 3D microelectrode arrays for in vitro and in vivo neuronal tissue recordings. *Adv. Sci.* **11**, 2305944 (2024).
65. Williams, J. C., Rennaker, R. L. & Kipke, D. R. Long-term neural recording characteristics of wire microelectrode arrays implanted in cerebral cortex. *Brain Res. Protoc.* **4**, 303–313 (1999).

66. Patel, P. R. et al. Insertion of linear 8.4 µm diameter 16 channel carbon fiber electrode arrays for single unit recordings. *J. Neural Eng.* **12**, 046009 (2015).
67. Andres, C. et al. Multifunctional fibers for simultaneous optical, electrical and chemical interrogation of neural circuits in vivo. *Nat. Biotechnol.* **33**, 273–284 (2015).
68. Bahar, G. M. & Mohamad, S. Design and implementation challenges of microelectrode arrays: a review. *Mater. Sci. Appl.* **04**, 483–495 (2013).
69. Yi, D., Yao, Y., Wang, Y. & Chen, L. Manufacturing processes of implantable microelectrode array for in vivo neural electrophysiological recordings and stimulation: a state-of-the-art review. *J. Micro Nano Manuf.* **10**, 041001 (2022).
70. Canales, A., Park, S., Kilias, A. & Anikeeva, P. Multifunctional fibers as tools for neuroscience and neuroengineering. *Acc. Chem. Res.* **51**, 829–838 (2018).
71. Hejazi, M., Tong, W., Ibbotson, M. R., Prawer, S. & Garrett, D. J. Advances in carbon-based microfiber electrodes for neural interfacing. *Front. Neurosci.* **15**, 658703 (2021).
72. Patil, A. C. & Thakor, N. V. Implantable neurotechnologies: a review of micro- and nanoelectrodes for neural recording. *Med. Biol. Eng. Comput.* **54**, 23–44 (2016).
73. Ganji, M. et al. Selective formation of porous Pt nanorods for highly electrochemically efficient neural electrode interfaces. *Nano Lett.* **19**, 6244–6254 (2019).
74. Weiland, J. D. & Anderson, D. J. Chronic neural stimulation with thin-film, iridium oxide electrodes. *IEEE Trans. Biomed. Eng.* **47**, 911–918 (2000).
75. Cui, X. & Martin, D. C. Electrochemical deposition and characterization of poly (3,4-ethylenedioxythiophene) on neural microelectrode arrays. *Sens. Actuators B Chem.* **89**, 92–102 (2003).
76. Oldroyd, P., Gurke, J. & Malliaras, G. G. Stability of thin film neuromodulation electrodes under accelerated aging conditions. *Adv. Funct. Mater.* **33**, 2208881 (2023).
77. Schulte, J., Ashouri, D. & Stieglitz, T. The longevity of neural interfaces — mechanical oscillation of thin film metal-based neural electrodes determine stability during electrical stimulation. *Adv. Funct. Mater.* **34**, 2310130 (2024).
78. Levitt, J. B., Kiper, D. C. & Movshon, J. A. Receptive fields and functional architecture of macaque V2. *J. Neurophysiol.* **71**, 2517–2542 (1994).
79. Barriga-Rivera, A., Tatarinoff, V., Lovell, N. H., Morley, J. W. & Suaning, G. J. Long-term anesthetic protocol in rats: feasibility in electrophysiology studies in visual prosthesis. *Vet. Ophthalmol.* **21**, 290–297 (2018).
80. Callaway, E. M. Neural substrates within primary visual cortex for interactions between parallel visual pathways. *Prog. Brain Res.* **149**, 59–64 (2005).
81. Chen, S. et al. Brain-wide neural activity underlying memory-guided movement. *Cell* **187**, 676–691.e16 (2024).
82. Kundu, A., Wirenfeldt, M., Harreby, K. R. & Jensen, W. Biosafety assessment of an intra-neural electrode (TIME) following sub-chronic implantation in the median nerve of Göttingen minipigs. *Int. J. Artif. Organs* **37**, 466–476 (2014).
83. Herwik, S. et al. Fabrication technology for silicon-based microprobe arrays used in acute and sub-chronic neural recording. *J. Micromech. Microeng.* **19**, 074008 (2009).
84. Mahmoudian, B. et al. A method for chronic and semi-chronic microelectrode array implantation in deep brain structures using image guided neuronavigation. *J. Neurosci. Methods* **397**, 109948 (2023).
85. Drager, U. C. & Hubel, D. H. Responses to visual stimulation and relationship between visual, auditory, and somatosensory inputs in mouse superior colliculus. *J. Neurophysiol.* **38**, 690–713 (1975).
86. Antonini, A., Fagiolini, M. & Stryker, M. P. Anatomical correlates of functional plasticity in mouse visual cortex. *J. Neurosci.* **19**, 4388–4406 (1999).
87. Allen, W. E. et al. Thirst regulates motivated behavior through modulation of brainwide neural population dynamics. *Science* **364**, eaav3932 (2019).
88. Steinmetz, N. A., Zatka-Haas, P., Carandini, M. & Harris, K. D. Distributed coding of choice, action and engagement across the mouse brain. *Nature* **576**, 266–273 (2019).
89. Stringer, C., Pachitariu, M., Steinmetz, N., Carandini, M. & Harris, K. D. High-dimensional geometry of population responses in visual cortex. *Nature* **571**, 361–365 (2019).
90. Sorrenti, V. et al. Understanding the effects of anesthesia on cortical electrophysiological recordings: a scoping review. *Int. J. Mol. Sci.* **22**, 1286 (2021).
91. Schoonover, C. E., Ohashi, S. N., Axel, R. & Fink, A. J. P. Representational drift in primary olfactory cortex. *Nature* **594**, 541–546 (2021).
92. Chung, J., Sharif, F., Jung, D., Kim, S. & Royer, S. Micro-drive and headgear for chronic implant and recovery of optoelectronic probes. *Sci. Rep.* **7**, 2773 (2017).
93. Márton, G. et al. A silicon-based microelectrode array with a microdrive for monitoring brainstem regions of freely moving rats. *J. Neural Eng.* **13**, 026025 (2016).
94. Fee, M. S. & Leonardo, A. Miniature motorized microdrive and commutator system for chronic neural recording in small animals. *J. Neurosci. Methods* **112**, 83–94 (2001).
95. Korshunov, V. A. Miniature microdrive-headstage assembly for extracellular recording of neuronal activity with high-impedance electrodes in freely moving mice. *J. Neurosci. Methods* **158**, 179–185 (2006).
96. Vandecasteele, M. et al. Large-scale recording of neurons by movable silicon probes in behaving rodents. *J. Vis. Exp.* **61**, e3568 (2012).
97. Wilson, M. A. & McNaughton, B. L. Dynamics of the hippocampal ensemble code for space. *Science* **261**, 1055–1058 (1993).
98. Yamamoto, J. & Wilson, M. A. Large-scale chronically implantable precision motorized microdrive array for freely behaving animals. *J. Neurophysiol.* **100**, 2430–2440 (2008).
99. Vöröslakos, V., Petersen, P. C., Vöröslakos, B. & Buzsáki, G. Metal microdrive and head cap system for silicon probe recovery in freely moving rodent. *eLife* **10**, e65859 (2021).
100. Yamashita, K. et al. A floating 5-µm-diameter needle-electrode on the tissue for damage-reduced chronic neuronal recording in mice. *Lab Chip* https://doi.org/10.1039/D1LC01031J (2022).
101. Thompson, C. H. et al. Toward guiding principles for the design of biologically-integrated electrodes for the central nervous system. *J. Neural Eng.* **17**, 021001 (2020).
102. Thelin, J. et al. Implant size and fixation mode strongly influence tissue reactions in the CNS. *PLoS ONE* **6**, e12267 (2020).
103. Erofeev, A., Antifeev, I., Bolshakova, A., Bezprozvanny, I. & Vlasova, O. In vivo penetrating microelectrodes for brain electrophysiology. *Sensors* **22**, 9085 (2022).
104. Lewis, C. M. et al. Recording quality is systematically related to electrode impedance. *Adv. Healthc. Mater.* **13**, 2303401 (2024).
105. Huszár, R., Zhang, Y., Blockus, H. & Buzsáki, G. Preconfigured dynamics in the hippocampus are guided by embryonic birthdate and rate of neurogenesis. *Nat. Neurosci.* **25**, 1201–1212 (2022).
106. Lin, L. et al. Large-scale neural ensemble recording in the brains of freely behaving mice. *J. Neurosci. Methods* **155**, 28–38 (2006).
107. Navarro, X. et al. A critical review of interfaces with the peripheral nervous system for the control of neuroprostheses and hybrid bionic systems. *J. Peripher. Nerv. Syst.* **10**, 229–258 (2005).
108. Nielsen, T. N., Kurstjens, G. A. M. & Struijk, J. J. Transverse versus longitudinal tripolar configuration for selective stimulation with multipolar cuff electrodes. *IEEE Trans. Biomed. Eng.* **58**, 913–919 (2011).
109. Lertmanorat, Z., Gustafson, K. J. & Durand, D. M. Electrode array for reversing the recruitment order of peripheral nerve stimulation: experimental studies. *Ann. Biomed. Eng.* **34**, 152–160 (2006).
110. Boretius, T. et al. A transverse intrafascicular multichannel electrode (TIME) to interface with the peripheral nerve. *Biosens. Bioelectron.* **26**, 62–69 (2010).
111. Lawrence, S. M., Dhillon, G. S., Jensen, W., Yoshida, K. & Horch, K. W. Acute peripheral nerve recording characteristics of polymer-based longitudinal intrafascicular electrodes. *IEEE Trans. Neural Syst. Rehabil. Eng.* **12**, 345–348 (2004).
112. Rochford, A. E. et al. Functional neurological restoration of amputated peripheral nerve using biohybrid regenerative bioelectronics. *Sci. Adv.* **9**, eadd8162 (2023).
113. Wise, K. D., Angell, J. B. & Starr, A. An integrated-circuit approach to extracellular microelectrodes. *IEEE Trans. Biomed. Eng.* **17**, 238–247 (1970).
114. Bhandari, R., Negi, S., Rieth, L., Normann, R. A. & Solzbacher, F. A novel method of fabricating convoluted shaped electrode arrays for neural and retinal prostheses. *Sens. Actuators Phys.* **145–146**, 123–130 (2008).
115. Ho, M.-H., Chen, H., Tseng, F., Yeh, S.-R. & Lu, M. S.-C. CMOS micromachined probes by die-level fabrication for extracellular neural recording. *J. Micromech. Microeng.* **17**, 283 (2007).
116. Ribeiro, J. F., Boi, F., Lecomte, A., Angotzi, G. N. & Berdondini, L. Bioelectrodes for high-channel count and small form factor CMOS neural probes. In 2021 *10th International IEEE/EMBS Conference on Neural Engineering (NER)* 388–391 (IEEE, 2021).
117. Hassler, C., Boretius, T. & Stieglitz, T. Polymers for neural implants. *J. Polym. Sci. Part B Polym. Phys.* **49**, 18–33 (2011).
118. Buzsáki, G. & Schomburg, E. W. What does gamma coherence tell us about inter-regional neural communication? *Nat. Neurosci.* **18**, 484–489 (2015).
119. Lopez, C. M. & Huang, X. Circuits and architectures for neural recording interfaces. in *Biomedical Electronics, Noise Shaping ADCs, and Frequency References: Advances in Analog Circuit Design 2022* (eds Harpe, P., Baschirotto, A. & Makinwa, K. A. A.) 45–57 (Springer International Publishing, 2023).
120. Harrison, R. R. & Charles, C. A low-power low-noise CMOS amplifier for neural recording applications. *IEEE J. Solid State Circuits* **38**, 958–965 (2003).
121. Seymour, J. P., Wu, F., Wise, K. D. & Yoon, E. State-of-the-art MEMS and microsystem tools for brain research. *Microsyst. Nanoeng.* **3**, 1–16 (2017).
122. Mathis, A. et al. DeepLabCut: markerless pose estimation of user-defined body parts with deep learning. *Nat. Neurosci.* **21**, 1281–1289 (2018).
123. Wilms, C. SciMethods: controlling and coordinating experiments in neurophysiology. *Scientifica* https://www.scientifica.uk.com/learning-zone/scimethods-controlling-and-coordinating-experiments-in-neurophysiology (2025).
124. Dagher, S. & Ishiyama, S. Protocol for precise signal synchronization of electrophysiology, videography, and audio recordings using a custom-made pulse generator. *STAR Protoc.* **4**, 102306 (2023).
125. Open Ephys & Contributors. Synchronizing Data Streams. *Open Ephys* https://open-ephys.github.io/gui-docs/Tutorials/Data-Synchronization.html (2025).
126. Scallon, A. DAQ Synchronization. *Optogenetics and Neural Engineering Core* https://optogeneticsandneuralengineeringcore.gitlab.io/ONECoreSite/projects/DAQSyncro/DAQSyncronization/ (2021).
127. Keller, D., Erö, C. & Markram, H. Cell densities in the mouse brain: a systematic review. *Front. Neuroanat.* https://doi.org/10.3389/fnana.2018.00083 (2018).
128. Erö, C., Gewaltig, M.-O., Keller, D. & Markram, H. A cell atlas for the mouse brain. *Front. Neuroinform.* **12**, 84 (2018).
129. Oliveira, L. M. & Dimitrov, D. in *Methods for Neural Ensemble Re*cordings 2nd edn (ed. Nicolelis, M. A. L.) Ch. 2, 21–46 (CRC Press & Taylor & Francis, 2008).
130. Vöröslakos, M. et al. 3D-printed recoverable microdrive and base plate system for rodent electrophysiology. *Bio Protoc.* **11**, e4137 (2021).
131. Bimbard, C. et al. An adaptable, reusable, and light implant for chronic Neuropixels probes. *eLife* https://doi.org/10.7554/eLife.98522.2 (2025).
132. Yin, R. et al. Chronic co-implantation of ultraflexible neural electrodes and a cranial window. *Neurophotonics* **9**, 032204 (2022).
133. Felix, S. H. et al. Insertion of flexible neural probes using rigid stiffeners attached with biodissolvable adhesive. *J. Vis. Exp.* **79**, e50609 (2013).

134. Russell, W. M. S., Burch, R. L. & Hume, C. W. *The Principles of Humane Experimental Technique* Vol. 238 (Methuen London, 1959).
135. Festing, M. F. On determining sample size in experiments involving laboratory animals. *Lab Anim.* **52**, 341–350 (2018).
136. Gaskill, B. N. & Garner, J. P. Power to the people: power, negative results and sample size. *J. Am. Assoc. Lab. Anim. Sci.* **59**, 9–16 (2020).
137. Dell, R. B., Holleran, S. & Ramakrishnan, R. Sample size determination. *ILAR J.* **43**, 207–213 (2002).
138. Siegle, J. H. et al. Open Ephys: an open-source, plugin-based platform for multichannel electrophysiology. *J. Neural Eng.* **14**, 045003 (2017).
139. Oostenveld, R., Fries, P., Maris, E. & Schoffelen, J.-M. FieldTrip: open source software for advanced analysis of MEG, EEG, and invasive electrophysiological data. *Comput. Intell. Neurosci.* **2011**, 156869 (2011).
140. Buccino, A. P. et al. SpikeInterface, a unified framework for spike sorting. *eLife* **9**, e61834 (2020).
141. Brette, R. & Destexhe, A. (eds) *Handbook of Neural Activity Measurement* (Cambridge Univ. Press, 2012).
142. Harris, K. D., Henze, D. A., Csicsvari, J., Hirase, H. & Buzsáki, G. Accuracy of tetrode spike separation as determined by simultaneous intracellular and extracellular measurements. *J. Neurophysiol.* **84**, 401–414 (2000).
143. Jäckel, D., Frey, U., Fiscella, M., Franke, F. & Hierlemann, A. Applicability of independent component analysis on high-density microelectrode array recordings. *J. Neurophysiol.* **108**, 334–348 (2012).
144. Pachitariu, M., Sridhar, S., Pennington, J. & Stringer, C. Spike sorting with Kilosort4. *Nat. Methods* **21**, 914–921 (2024).
145. Shimazaki, H. & Shinomoto, S. A method for selecting the bin size of a time histogram. *Neural Comput.* **19**, 1503–1527 (2007).
146. Kass, R. E., Ventura, V. & Brown, E. N. Statistical issues in the analysis of neuronal data. *J. Neurophysiol.* **94**, 8–25 (2005).
147. Merchant, H., Naselaris, T. & Georgopoulos, A. P. Dynamic sculpting of directional tuning in the primate motor cortex during three-dimensional reaching. *J. Neurosci.* **28**, 9164–9172 (2008).
148. Mitchell, J. F., Sundberg, K. A. & Reynolds, J. H. Differential attention-dependent response modulation across cell classes in macaque visual area V4. *Neuron* **55**, 131–141 (2007).
149. Kaufman, M. T. et al. Roles of monkey premotor neuron classes in movement preparation and execution. *J. Neurophysiol.* **104**, 799–810 (2010).
150. Barthó, P. et al. Characterization of neocortical principal cells and interneurons by network interactions and extracellular features. *J. Neurophysiol.* **92**, 600–608 (2004).
151. Krimer, L. S. et al. Cluster analysis-based physiological classification and morphological properties of inhibitory neurons in layers 2–3 of monkey dorsolateral prefrontal cortex. *J. Neurophysiol.* **94**, 3009–3022 (2005).
152. Reich, D. S., Mechler, F., Purpura, K. P. & Victor, J. D. Interspike intervals, receptive fields, and information encoding in primary visual cortex. *J. Neurosci.* **20**, 1964–1974 (2000).
153. Gabbiani, F. & Koch, C. in *Methods in Neuronal Modeling* 2nd edn 313–360 (MIT Press, 1998).
154. Ostojic, S., Brunel, N. & Hakim, V. How connectivity, background activity, and synaptic properties shape the cross-correlation between spike trains. *J. Neurosci.* **29**, 10234–10235 (2009).
155. Szél, A., Martínez-Bellver, S., Hegedüs, P. & Hangya, B. OPETH: open source solution for real-time peri-event time histogram based on Open Ephys. *Front. Neuroinform.* **14**, 21 (2020).
156. Umakantha, A. et al. Bridging neuronal correlations and dimensionality reduction. *Neuron* **109**, 2740–2754.e12 (2021).
157. Williamson, R. C. et al. Scaling properties of dimensionality reduction for neural populations and network models. *PLoS Comput. Biol.* **12**, e1005141 (2016).
158. Cunningham, J. P. & Yu, B. M. Dimensionality reduction for large-scale neural recordings. *Nat. Neurosci.* **17**, 1500–1509 (2014).
159. Angotzi, G. N. et al. Multi-shank 1024 channels active SiNAPS probe for large multi-regional topographical electrophysiological mapping of neural dynamics. Preprint at *Res. Sq.* https://doi.org/10.21203/rs.3.rs-4800131/v1 (2024).
160. Lewis, C. M., Bosman, C. A. & Fries, P. Recording of brain activity across spatial scales. *Curr. Opin. Neurobiol.* **32**, 68–77 (2015).
161. Bizley, J. K., Nodal, F. R., Bajo, V. M., Nelken, I. & King, A. J. Physiological and anatomical evidence for multisensory interactions in auditory cortex. *Cereb. Cortex* **17**, 2172–2189 (2007).
162. Lakatos, P., Chen, C.-M., O'Connell, M. N., Mills, A. & Schroeder, C. E. Neuronal oscillations and multisensory interaction in primary auditory cortex. *Neuron* **53**, 279–292 (2007).
163. Reed, J. L. et al. Widespread spatial integration in primary somatosensory cortex. *Proc. Natl Acad. Sci. USA* **105**, 10233–10237 (2008).
164. Bolding, K. A. & Franks, K. M. Complementary codes for odor identity and intensity in olfactory cortex. *eLife* **6**, e22630 (2017).
165. Lavaud, S., D'Andola, M., Bichara, C. & Takeoka, A. Electrophysiological signatures reveal spinal learning mechanisms for a lasting sensorimotor adaptation. Preprint at *bioRxiv* https://doi.org/10.1101/2022.03.30.486422 (2022).
166. Chapin, J. K. Using multi-neuron population recordings for neural prosthetics. *Nat. Neurosci.* **7**, 452–455 (2004).
167. Georgopoulos, A. P., Kalaska, J. F., Caminiti, R. & Massey, J. T. On the relations between the direction of two-dimensional arm movements and cell discharge in primate motor cortex. *J. Neurosci.* **2**, 1527–1537 (1982).
168. Moran, D. W. & Schwartz, A. B. Motor cortical representation of speed and direction during reaching. *J. Neurophysiol.* **82**, 2676–2692 (1999).
169. Gilja, V. et al. A high-performance neural prosthesis enabled by control algorithm design. *Nat. Neurosci.* **15**, 1752–1757 (2012).
170. Georgopoulos, A. P., Schwartz, A. B. & Kettner, R. E. Neuronal population coding of movement direction. *Science* **233**, 1416–1419 (1986).
171. Wessberg, J. et al. Real-time prediction of hand trajectory by ensembles of cortical neurons in primates. *Nature* **408**, 361–365 (2000).
172. Chase, S. M., Schwartz, A. B. & Kass, R. E. Bias, optimal linear estimation, and the differences between open-loop simulation and closed-loop performance of spiking-based brain–computer interface algorithms. *Neural Netw.* **22**, 1203–1213 (2009).
173. Carmena, J. M. et al. Learning to control a brain-machine interface for reaching and grasping by primates. *PLoS Biol.* **1**, E42 (2003).
174. Velliste, M., Perel, S., Spalding, M. C., Whitford, A. S. & Schwartz, A. B. Cortical control of a prosthetic arm for self-feeding. *Nature* **453**, 1098–1101 (2008).
175. Pandarinath, C. & Bensmaia, S. J. The science and engineering behind sensitized brain-controlled bionic hands. *Physiol. Rev.* **102**, 551–604 (2022).
176. Fernández, E. et al. Visual percepts evoked with an intracortical 96-channel microelectrode array inserted in human occipital cortex. *J. Clin. Invest.* **131**, e151331 (2021).
177. O'Keefe, J. & Dostrovsky, J. The hippocampus as a spatial map. Preliminary evidence from unit activity in the freely-moving rat. *Brain Res.* **34**, 171–175 (1971).
178. Hafting, T., Fyhn, M., Molden, S., Moser, M.-B. & Moser, E. I. Microstructure of a spatial map in the entorhinal cortex. *Nature* **436**, 801–806 (2005).
179. Buzsáki, G. Hippocampal sharp wave-ripple: a cognitive biomarker for episodic memory and planning. *Hippocampus* **25**, 1073–1188 (2015).
180. Kovacs, G. T. A., Storment, C. W. & Rosen, J. M. Regeneration microelectrode array for peripheral nerve recording and stimulation. *IEEE Trans. Biomed. Eng.* **39**, 893–902 (1992).
181. Ordonez, J., Schuettler, M., Boehler, C., Boretius, T. & Stieglitz, T. Thin films and microelectrode arrays for neuroprosthetics. *MRS Bull.* **37**, 590–598 (2012).
182. Sinkjær, T., Haugland, M. & Haase, J. Natural neural sensing and artificial muscle control in man. *Exp. Brain Res.* **98**, 542–545 (1994).
183. Inmann, A., Haugland, M., Haase, J., Biering-Sørensen, F. & Sinkjaer, T. Signals from skin mechanoreceptors used in control of a hand grasp neuroprosthesis. *Neuroreport* **12**, 2817–2820 (2001).
184. Cracchiolo, M. et al. Decoding of grasping tasks from intraneural recordings in trans-radial amputee. *J. Neural Eng.* **17**, 026034 (2020).
185. Taylor, J., Schuettler, M., Clarke, C. & Donaldson, N. The theory of velocity selective neural recording: a study based on simulation. *Med. Biol. Eng. Comput.* **50**, 309–318 (2012).
186. Schuettler, M., Donaldson, N., Seetohul, V. & Taylor, J. Fibre-selective recording from the peripheral nerves of frogs using a multi-electrode cuff*. *J. Neural Eng.* **10**, 036016 (2013).
187. Clarke, C., Rieger, R., Schuettler, M., Donaldson, N. & Taylor, J. An implantable ENG detector with in-system velocity selective recording (VSR) capability. *Med. Biol. Eng. Comput.* **55**, 885–895 (2017).
188. Pasluosta, C. et al. Bidirectional bionic limbs: a perspective bridging technology and physiology. *J. Neural Eng.* **19**, 013001 (2022).
189. Raspopovic, S., Valle, G. & Petrini, F. M. Sensory feedback for limb prostheses in amputees. *Nat. Mater.* **20**, 925–939 (2021).
190. Bensmaia, S. J. Biological and bionic hands: natural neural coding and artificial perception. *Philos. Trans. R. Soc. Lond. B. Biol. Sci.* **370**, 20140209 (2015).
191. Tan, D. W. et al. A neural interface provides long-term stable natural touch perception. *Sci. Transl. Med.* **6**, 257ra138 (2014).
192. Petrini, F. M. et al. Sensory feedback restoration in leg amputees improves walking speed, metabolic cost and phantom pain. *Nat. Med.* **25**, 1356–1363 (2019).
193. Raspopovic, S. et al. Restoring natural sensory feedback in real-time bidirectional hand prostheses. *Sci. Transl. Med.* **6**, 222ra19 (2014).
194. Rossini, P. M. et al. Double nerve intraneural interface implant on a human amputee for robotic hand control. *Clin. Neurophysiol.* **121**, 777–783 (2010).
195. Dhillon, G. S. & Horch, K. W. Direct neural sensory feedback and control of a prosthetic arm. *IEEE Trans. Neural Syst. Rehabil. Eng.* **13**, 468–472 (2005).
196. Larson, C. E. & Meng, E. A review for the peripheral nerve interface designer. *J. Neurosci. Methods* **332**, 108523 (2020).
197. Brindley, G. S. The first 500 patients with sacral anterior root stimulator implants: general description. *Paraplegia* **32**, 795–805 (1994).
198. Creasey, G. H. Electrical stimulation of sacral roots for micturition after spinal cord injury. *Urol. Clin. North. Am.* **20**, 505–515 (1993).
199. Dimitrijevic, M. R., Danner, S. M. & Mayr, W. Neurocontrol of movement in humans with spinal cord injury. *Artif. Organs* **39**, 823–833 (2015).
200. Guiraud, D., Stieglitz, T., Koch, K. P., Divoux, J.-L. & Rabischong, P. An implantable neuroprosthesis for standing and walking in paraplegia: 5-year patient follow-up. *J. Neural Eng.* **3**, 268–275 (2006).
201. Burridge, J. H. et al. Patients' perceptions of the benefits and problems of using the ActiGait implanted drop-foot stimulator. *J. Rehabil. Med.* **40**, 873–875 (2008).

202. Martin, D., Patriciu, A., Schulz, A.-K. & Schackert, G. Long-term results following electrical stimulation of the peroneal nerve using the ActiGait® system in 33 patients with central drop foot. *Innov. Surg. Sci.* **6**, 3–9 (2021).
203. Severinsen, K. et al. Implanted peroneal nerve stimulator treatment for drop foot caused by central nervous system lesion: a twelve-month follow-up of 21 patients. *J. Rehabil. Med.* **54**, jrm00288 (2022).
204. Hoffer, J. A. et al. Neural signals for command control and feedback in functional neuromuscular stimulation: a review. *J. Rehabil. Res. Dev.* **33**, 145–157 (1996).
205. Haugland, M. et al. Restoration of lateral hand grasp using natural sensors. *Artif. Organs* **21**, 250–253 (1997).
206. Haugland, M., Lickel, A., Haase, J. & Sinkjaer, T. Control of FES thumb force using slip information obtained from the cutaneous electroneurogram in quadriplegic man. *IEEE Trans. Rehabil. Eng.* **7**, 215–227 (1999).
207. Hansen, M., Haugland, M., Sinkjaer, T. & Donaldson, N. Real time foot drop correction using machine learning and natural sensors. *Neuromodul. J. Int. Neuromodul. Soc.* **5**, 41–53 (2002).
208. Farina, D. et al. Toward higher-performance bionic limbs for wider clinical use. *Nat. Biomed. Eng.* **7**, 473–485 (2023).
209. Vallbo, Å. B. Microneurography: how it started and how it works. *J. Neurophysiol.* **120**, 1415–1427 (2018).
210. Farina, D., Yoshida, K., Stieglitz, T. & Koch, K. P. Multichannel thin-film electrode for intramuscular electromyographic recordings. *J. Appl. Physiol. Bethesda MD 1985* **104**, 821–827 (2008).
211. Negredo, P., Castro, J., Lago, N., Navarro, X. & Avendaño, C. Differential growth of axons from sensory and motor neurons through a regenerative electrode: a stereological, retrograde tracer, and functional study in the rat. *Neuroscience* **128**, 605–615 (2004).
212. Boehler, C., Carli, S., Fadiga, L., Stieglitz, T. & Asplund, M. Tutorial: guidelines for standardized performance tests for electrodes intended for neural interfaces and bioelectronics. *Nat. Protoc.* **15**, 3557–3578 (2020).
213. Prasad, A. & Sanchez, J. C. Quantifying long-term microelectrode array functionality using chronic in vivo impedance testing. *J. Neural Eng.* **9**, 026028 (2012).
214. Buzsáki, G. Large-scale recording of neuronal ensembles. *Nat. Neurosci.* **7**, 446–451 (2004).
215. Henze, D. A. et al. Intracellular features predicted by extracellular recordings in the hippocampus in vivo. *J. Neurophysiol.* **84**, 390–400 (2000).
216. Kozai, T. D. Y. et al. Comprehensive chronic laminar single-unit, multi-unit, and local field potential recording performance with planar single shank electrode arrays. *J. Neurosci. Methods* **242**, 15–40 (2015).
217. International Brain Laboratory et al. Reproducibility of in vivo electrophysiological measurements in mice. *eLife* https://doi.org/10.7554/eLife.100840.1 (2025).
218. Fraser, G. W. & Schwartz, A. B. Recording from the same neurons chronically in motor cortex. *J. Neurophysiol.* **107**, 1970–1978 (2011).
219. Fu, T.-M. et al. Stable long-term chronic brain mapping at the single-neuron level. *Nat. Methods* **13**, 875–882 (2016).
220. Percie du Sert, N. et al. The ARRIVE guidelines 2.0: updated guidelines for reporting animal research*. *J. Cereb. Blood Flow Metab.* **40**, 1769–1777 (2020).
221. Magland, J. et al. SpikeForest, reproducible web-facing ground-truth validation of automated neural spike sorters. *eLife* **9**, e55167 (2020).
222. Birman, D. et al. Interactive data exploration websites for large-scale electrophysiology. Preprint at *bioRxiv* https://doi.org/10.1101/2024.06.07.597950 (2024).
223. Ghosh, K. K. et al. Miniaturized integration of a fluorescence microscope. *Nat. Methods* **8**, 871–878 (2011).
224. Zong, W. et al. Large-scale two-photon calcium imaging in freely moving mice. *Cell* **185**, 1240–1256.e30 (2022).
225. Wu, F. et al. Monolithically integrated µLEDs on silicon neural probes for high-resolution optogenetic studies in behaving animals. *Neuron* **88**, 1136–1148 (2015).
226. Wiltschko, A. B. et al. Mapping sub-second structure in mouse behavior. *Neuron* **88**, 1121–1135 (2015).
227. Rübel, O. et al. The neurodata without borders ecosystem for neurophysiological data science. *eLife* **11**, e78362 (2022).
228. De Smedt, K., Koureas, D. & Wittenburg, P. FAIR digital objects for science: from data pieces to actionable knowledge units. *Publications* **8**, 21 (2020).
229. Kozai, T. D. Y. & Vazquez, A. L. Photoelectric artefact from optogenetics and imaging on microelectrodes and bioelectronics: new challenges and opportunities. *J. Mater. Chem. B* **3**, 4965–4978 (2015).
230. Kim, K. et al. Artifact-free and high-temporal-resolution in vivo opto-electrophysiology with microLED optoelectrodes. *Nat. Commun.* **11**, 2063 (2020).
231. Young, D. et al. Signal processing methods for reducing artifacts in microelectrode brain recordings caused by functional electrical stimulation. *J. Neural Eng.* **15**, 026014 (2018).
232. O'Shea, D. J. & Shenoy, K. V. ERAASR: an algorithm for removing electrical stimulation artifacts from multielectrode array recordings. *J. Neural Eng.* **15**, 026020 (2018).
233. Campbell, A. & Wu, C. Chronically implanted intracranial electrodes: tissue reaction and electrical changes. *Micromachines* **9**, 430 (2018).
234. Carnicer-Lombarte, A., Chen, S.-T., Malliaras, G. G. & Barone, D. G. Foreign body reaction to implanted biomaterials and its impact in nerve neuroprosthetics. *Front. Bioeng. Biotechnol.* **9**, 622524 (2021).
235. Du, Z. J. et al. Ultrasoft microwire neural electrodes improve chronic tissue integration. *Acta Biomater.* **53**, 46–58 (2017).
236. Barrese, J. C., Aceros, J. & Donoghue, J. P. Scanning electron microscopy of chronically implanted intracortical microelectrode arrays in non-human primates. *J. Neural Eng.* **13**, 026003 (2016).
237. Sponheim, C. et al. Longevity and reliability of chronic unit recordings using the Utah, intracortical multi-electrode arrays. *J. Neural Eng.* https://doi.org/10.1088/1741-2552/ac3eaf (2021).
238. Luo, T. Z. et al. An approach for long-term, multi-probe Neuropixels recordings in unrestrained rats. *eLife* **9**, e59716 (2020).
239. Kozai, T. D. Y. et al. Chronic tissue response to carboxymethyl cellulose based dissolvable insertion needle for ultra-small neural probes. *Biomaterials* **35**, 9255–9268 (2014).
240. Kozai, T. D. Y., Jaquins-Gerstl, A. S., Vazquez, A. L., Michael, A. C. & Cui, X. T. Brain tissue responses to neural implants impact signal sensitivity and intervention strategies. *ACS Chem. Neurosci.* **6**, 48–67 (2015).
241. Golabchi, A., Wu, B., Cao, B., Bettinger, C. J. & Cui, X. T. Zwitterionic polymer/polydopamine coating reduce acute inflammatory tissue responses to neural implants. *Biomaterials* **225**, 119519 (2019).
242. Wu, B. et al. Zwitterionic polymer coated and aptamer functionalized flexible micro-electrode arrays for in vivo cocaine sensing and electrophysiology. *Micromachines* **14**, 323 (2023)
243. Harris, J. P. et al. In vivo deployment of mechanically adaptive nanocomposites for intracortical microelectrodes. *J. Neural Eng.* **8**, 046010 (2011).
244. Chung, J. E. et al. High-density, long-lasting, and multi-region electrophysiological recordings using polymer electrode arrays. *Neuron* **101**, 21–31.e5 (2019).
245. Golabchi, A. et al. Melatonin improves quality and longevity of chronic neural recording. *Biomaterials* **180**, 225–239 (2018).
246. Golabchi, A., Woeppel, K. M., Li, X., Lagenaur, C. F. & Cui, X. T. Neuroadhesive protein coating improves the chronic performance of neuroelectronics in mouse brain. *Biosens. Bioelectron.* **155**, 112096 (2020).
247. Shi, D., Narayanan, S., Woeppel, K. & Cui, X. T. Improving the biocompatibility and functionality of neural interface devices with silica nanoparticles. *Acc. Chem. Res.* **57**, 1684–1695 (2024).
248. Asplund, M., Boehler, C. & Stieglitz, T. Anti-inflammatory polymer electrodes for glial scar treatment: bringing the conceptual idea to future results. *Front. Neuroeng.* **7**, 9 (2014).
249. Boehler, C., Oberueber, F. & Asplund, M. Tuning drug delivery from conducting polymer films for accurately controlled release of charged molecules. *J. Controlled Rel.* **304**, 173–180 (2019).
250. Golabchi, A., Wu, B., Du, Z. J. & Cui, X. T. Long-term neural recording performance of PEDOT/CNT/dexamethasone-coated electrode array implanted in visual cortex of rats. *Adv. NanoBiomed Res.* **5**, 2400114 (2025).
251. Eles, J. R. et al. Neuroadhesive L1 coating attenuates acute microglial attachment to neural electrodes as revealed by live two-photon microscopy. *Biomaterials* **113**, 279–292 (2017).
252. Kolarcik, C. L. et al. In vivo effects of L1 coating on inflammation and neuronal health at the electrode–tissue interface in rat spinal cord and dorsal root ganglion. *Acta Biomater.* **8**, 3561–3575 (2012).
253. Azemi, E., Lagenaur, C. F. & Cui, X. T. The surface immobilization of the neural adhesion molecule L1 on neural probes and its effect on neuronal density and gliosis at the probe/tissue interface. *Biomaterials* **32**, 681–692 (2011).
254. Azemi, E., Stauffer, W. R., Gostock, M. S., Lagenaur, C. F. & Cui, X. T. Surface immobilization of neural adhesion molecule L1 for improving the biocompatibility of chronic neural probes: in vitro characterization. *Acta Biomater.* **4**, 1208–1217 (2008).
255. Barrese, J. C. et al. Failure mode analysis of silicon-based intracortical microelectrode arrays in non-human primates. *J. Neural Eng.* **10**, 066014 (2013).
256. Wissel, K. et al. Platinum corrosion products from electrode contacts of human cochlear implants induce cell death in cell culture models. *PLoS ONE* **13**, e0196649 (2018).
257. Čvančara, P. et al. Stability of flexible thin-film metallization stimulation electrodes: analysis of explants after first-in-human study and improvement of in vivo performance. *J. Neural Eng.* **17**, 046006 (2020).
258. Čvančara, P. et al. Bringing sensation to prosthetic hands — chronic assessment of implanted thin-film electrodes in humans. *npj Flex. Electron.* **7**, 51 (2023).
259. Böhm, T. et al. Quantitative synchrotron X-ray tomography of the material-tissue interface in rat cortex implanted with neural probes. *Sci. Rep.* **9**, 7646 (2019).
260. Joseph, K. et al. Transcriptional characterization of the glial response due to chronic neural implantation of flexible microprobes. *Biomaterials* **279**, 121230 (2021).
261. Wellman, S. M. et al. A materials roadmap to functional neural interface design. *Adv. Funct. Mater.* **28**, 1701269 (2018).
262. Joshi-Imre, A. et al. Chronic recording and electrochemical performance of amorphous silicon carbide-coated Utah electrode arrays implanted in rat motor cortex. *J. Neural Eng.* **16**, 046006 (2019).
263. Beygi, M. et al. Fabrication of a monolithic implantable neural interface from cubic silicon carbide. *Micromachines* **10**, 430 (2019).
264. Deku, F. et al. Amorphous silicon carbide ultramicroelectrode arrays for neural stimulation and recording. *J. Neural Eng.* **15**, 016007 (2018).
265. Ahn, S.-H., Jeong, J. & Kim, S. J. Emerging encapsulation technologies for long-term reliability of microfabricated implantable devices. *Micromachines* **10**, 508 (2019).
266. Caldwell, R. et al. Failure mode analysis of $Al_2O_2$-parylene c bilayer encapsulation for implantable devices and application to penetrating neural arrays. In *2015 Transducers — 2015 18th International Conference on Solid-State Sensors, Actuators and Microsystems* (*TRANSDUCERS*) 1747–1750 (IEEE, 2015).

267. Mariello, M. et al. Hermetic, hybrid multilayer, sub-5μm-thick encapsulations prepared with vapor-phase infiltration of metal oxides in conformal polymers for flexible bioelectronics. *Adv. Funct. Mater.* **34**, 2403973 (2024).
268. Zheng, X. S., Tan, C., Castagnola, E. & Cui, X. T. Electrode materials for chronic electrical microstimulation. *Adv. Healthc. Mater.* **10**, 2100119 (2021).
269. Orlemann, C. et al. Flexible polymer electrodes for stable prosthetic visual perception in mice. *Adv. Healthc. Mater.* **13**, 2304169 (2024).
270. Lycke, R. et al. Low-threshold, high-resolution, chronically stable intracortical microstimulation by ultraflexible electrodes. *Cell Rep.* **42**, 112554 (2023).
271. He, F. et al. Longitudinal neural and vascular recovery following ultraflexible neural electrode implantation in aged mice. *Biomaterials* **291**, 121905 (2022).
272. Maikos, J. T., Elias, R. A. I. & Shreiber, D. I. Mechanical properties of dura mater from the rat brain and spinal cord. *J. Neurotrauma* **25**, 38–51 (2008).
273. Kozai, T. D. Y. et al. Reduction of neurovascular damage resulting from microelectrode insertion into the cerebral cortex using in vivo two-photon mapping. *J. Neural Eng.* **7**, 046011 (2010).
274. Sharpening. *GitHub* https://github.com/cortex-lab/neuropixels/wiki/Sharpening (2023).
275. Fiáth, R. et al. Slow insertion of silicon probes improves the quality of acute neuronal recordings. *Sci. Rep.* **9**, 111 (2019).
276. Na, K. et al. Novel diamond shuttle to deliver flexible neural probe with reduced tissue compression. *Microsyst. Nanoeng.* **6**, 37 (2020).
277. Kumosa, L. S. & Schouenborg, J. Profound alterations in brain tissue linked to hypoxic episode after device implantation. *Biomaterials* **278**, 121143 (2021).
278. Rousche, P. J. & Normann, R. A. A method for pneumatically inserting an array of penetrating electrodes into cortical tissue. *Ann. Biomed. Eng.* **20**, 413–422 (1992).
279. Thomas, W. M., Leber, M., Crew, J. & Warren, D. J. Evaluation of pneumatic insertion stability of Utah slanted electrode arrays in rat sciatic nerve. *Annu. Int. Conf. IEEE Eng. Med. Biol. Soc.* **2022**, 5099–5102 (2022).
280. Birman, D. et al. Pinpoint: trajectory planning for multi-probe electrophysiology and injections in an interactive web-based 3D environment. Preprint at *bioRxiv* https://doi.org/10.1101/2023.07.14.548952 (2023).
281. Blanche, T. J. & Swindale, N. V. Nyquist interpolation improves neuron yield in multiunit recordings. *J. Neurosci. Methods* **155**, 81–91 (2006).
282. Buccino, A. P. et al. Compression strategies for large-scale electrophysiology data. *J. Neural Eng.* **20**, 056009 (2023).
283. Ghouse, M., Li, M., Long, C. & Jiang, J. Multichannel extracellular recording in freely moving mice. *J. Vis. Exp.* https://doi.org/10.3791/65245 (2023).
284. Xie, K., Fox, G. E., Liu, J. & Tsien, J. Z. 512-channel and 13-region simultaneous recordings coupled with optogenetic manipulation in freely behaving mice. *Front. Syst. Neurosci.* **10**, 48 (2016).
285. Fan, D. et al. A wireless multi-channel recording system for freely behaving mice and rats. *PLoS ONE* **6**, e22033 (2011).
286. Gutruf, P. & Rogers, J. A. Implantable, wireless device platforms for neuroscience research. *Curr. Opin. Neurobiol.* **50**, 42–49 (2018).
287. Yang, Y. et al. Wireless multilateral devices for optogenetic studies of individual and social behaviors. *Nat. Neurosci.* **24**, 1035–1045 (2021).
288. Pinnell, R. C., Dempster, J. & Pratt, J. Miniature wireless recording and stimulation system for rodent behavioural testing. *J. Neural Eng.* **12**, 066015 (2015).
289. Morizio, J., Irazoqui, P., Go, V. & Parmentier, J. Wireless headstage for neural prosthetics. In *Conference Proc. 2nd International IEEE EMBS Conference on Neural Engineering* 414–417 (IEEE, 2005).
290. Even-Chen, N. et al. Power-saving design opportunities for wireless intracortical brain computer interfaces. *Nat. Biomed. Eng.* **4**, 984 (2020).
291. Ide, K. & Takahashi, S. A review of neurologgers for extracellular recording of neuronal activity in the brain of freely behaving wild animals. *Micromachines* **13**, 1529 (2022).
292. Malekoshoaraie, M. H. et al. Fully flexible implantable neural probes for electrophysiology recording and controlled neurochemical modulation. *Microsyst. Nanoeng.* **10**, 91 (2024).
293. Wu, B., Castagnola, E., McClung, C. A. & Cui, X. T. PEDOT/CNT flexible MEAs reveal new insights into the Clock gene's role in dopamine dynamics. *Adv. Sci.* **11**, e2308212 (2024).
294. Johnson, M. D., Kao, O. E. & Kipke, D. R. Spatiotemporal pH dynamics following insertion of neural microelectrode arrays. *J. Neurosci. Methods* **160**, 276–287 (2007).
295. Chung, H.-J. et al. Ultrathin, stretchable, multiplexing pH sensor arrays on biomedical devices with demonstrations on rabbit and human hearts undergoing ischemia. *Adv. Healthc. Mater.* **3**, 59–68 (2014).
296. Wang, J., Xie, H., Chung, T., Chan, L. L. H. & Pang, S. W. Neural probes with integrated temperature sensors for monitoring retina and brain implantation and stimulation. *IEEE Trans. Neural Syst. Rehabil. Eng.* **25**, 1663–1673 (2017).
297. Zhang, S. et al. Development of silicon probe with acute study on in vivo neural recording and implantation behavior monitored by integrated Si-nanowire strain sensors. *J. Microelectromech. Syst.* **24**, 1303–1313 (2015).
298. Xu, K. et al. Bioresorbable electrode array for electrophysiological and pressure signal recording in the brain. *Adv. Healthc. Mater.* **8**, 1801649 (2019).
299. Pang, C., Lee, C. & Suh, K.-Y. Recent advances in flexible sensors for wearable and implantable devices. *J. Appl. Polym. Sci.* **130**, 1429–1441 (2013).
300. Sullender, C. T., Richards, L. M., He, F., Luan, L. & Dunn, A. K. Dynamics of isoflurane-induced vasodilation and blood flow of cerebral vasculature revealed by multi-exposure speckle imaging. *J. Neurosci. Methods* **366**, 109434 (2022).
301. Park, D.-W. et al. Graphene-based carbon-layered electrode array technology for neural imaging and optogenetic applications. *Nat. Commun.* **5**, 5258 (2014).
302. Yang, Q. et al. Integrated microprism and microelectrode array for simultaneous electrophysiology and two-photon imaging across all cortical layers. *Adv. Healthc. Mater.* **13**, 2302362 (2024).
303. Dijk, G., Kaszas, A., Pas, J. & O'Connor, R. P. Fabrication and in vivo 2-photon microscopy validation of transparent PEDOT:PSS microelectrode arrays. *Microsyst. Nanoeng.* **8**, 1–8 (2022).
304. Koschinski, L. et al. Validation of transparent and flexible neural implants for simultaneous electrophysiology, functional imaging, and optogenetics. *J. Mater. Chem. B* **11**, 9639–9657 (2023).
305. Ramezani, M. et al. High-density transparent graphene arrays for predicting cellular calcium activity at depth from surface potential recordings. *Nat. Nanotechnol.* **19**, 504–513 (2024).
306. Wu, Y. et al. Ultraflexible electrodes for recording neural activity in the mouse spinal cord during motor behavior. *Cell Rep.* **43**, 114199 (2024).
307. Meacham, K. W., Giuly, R. J., Guo, L., Hochman, S. & DeWeerth, S. P. A lithographically-patterned, elastic multi-electrode array for surface stimulation of the spinal cord. *Biomed. Microdevices* **10**, 259–269 (2008).
308. Sperry, Z. J. et al. Flexible microelectrode array for interfacing with the surface of neural ganglia. *J. Neural Eng.* **15**, 036027 (2018).
309. Woodington, B. J. et al. X-ray markers for thin film implants. *Adv. Healthc. Mater.* **11**, 2200739 (2022).
310. Venton, B. J. & Cao, Q. Fundamentals of fast-scan cyclic voltammetry for dopamine detection. *Analyst* **145**, 1158–1168 (2020).
311. Kim, J. et al. Fabrication of high-performance ultrathin $In_2O_3$ film field-effect transistors and biosensors using chemical lift-off lithography. *ACS Nano* **9**, 4572–4582 (2015).
312. Romanholo, P. V. V. et al. Biomimetic electrochemical sensors: new horizons and challenges in biosensing applications. *Biosens. Bioelectron.* **185**, 113242 (2021).
313. Wu, B., Castagnola, E. & Cui, X. T. Zwitterionic polymer coated and aptamer functionalized flexible micro-electrode arrays for in vivo cocaine sensing and electrophysiology. *Micromachines* **14**, 323 (2023).
314. Taylor, I. M. et al. Aptamer-functionalized neural recording electrodes for the direct measurement of cocaine in vivo. *J. Mater. Chem. B* **5**, 2445–2458 (2017).
315. Wu, G. et al. Implantable aptamer-graphene microtransistors for real-time monitoring of neurochemical release in vivo. *Nano Lett.* **22**, 3668–3677 (2022).
316. Jiang, Y. & Tian, B. Inorganic semiconductor biointerfaces. *Nat. Rev. Mater.* **3**, 473–490 (2018).
317. Gao, Z. et al. Multiplexed monitoring of neurochemicals via electrografting-enabled site-selective functionalization of aptamers on field-effect transistors. *Anal. Chem.* **94**, 8605–8617 (2022).
318. Xie, K. et al. Organic electrochemical transistor arrays for real-time mapping of evoked neurotransmitter release in vivo. *eLife* **9**, e50345 (2020).
319. Cea, C. et al. Integrated internal ion-gated organic electrochemical transistors for stand-alone conformable bioelectronics. *Nat. Mater.* **22**, 1227–1235 (2023).
320. Li, N. et al. Bioadhesive polymer semiconductors and transistors for intimate biointerfaces. *Science* **381**, 686–693 (2023).
321. Khonina, S. N., Kazanskiy, N. L., Butt, M. A. & Karpeev, S. V. Optical multiplexing techniques and their marriage for on-chip and optical fiber communication: a review. *Opto-Electron. Adv.* **5**, 210127–25 (2022).
322. Woeppel, K. M., Zheng, X. S., Schulte, Z. M., Rosi, N. L. & Cui, X. T. Nanoparticle doped PEDOT for enhanced electrode coatings and drug delivery. *Adv. Healthc. Mater.* **8**, 1900622 (2019).
323. Tan, C., Kushwah, N. & Cui, X. T. Electrically controlled neurochemical delivery from microelectrodes for focal and transient modulation of cellular behavior. *Biosensors* **11**, 348 (2021).
324. Woeppel, K. M., Krahe, D. D., Robbins, E. M., Vazquez, A. L. & Cui, X. T. Electrically controlled vasodilator delivery from PEDOT/silica nanoparticle modulates vessel diameter in mouse brain. *Adv. Healthc. Mater.* **13**, 2301221 (2024).
325. Du, Z. J. et al. Electrically controlled neurochemical release from dual-layer conducting polymer films for precise modulation of neural network activity in rat barrel cortex. *Adv. Funct. Mater.* **28**, 1703988 (2017).
326. Huang, H., Delikanli, S., Zeng, H., Ferkey, D. M. & Pralle, A. Remote control of ion channels and neurons through magnetic-field heating of nanoparticles. *Nat. Nanotechnol.* **5**, 602–606 (2010).
327. He, D. et al. Noncovalent assembly of reduced graphene oxide and alkyl-grafted mesoporous silica: an effective drug carrier for near-infrared light-responsive controlled drug release. *J. Mater. Chem. B* **3**, 5588–5594 (2015).
328. Bar-Zion, A. et al. Acoustically triggered mechanotherapy using genetically encoded gas vesicles. *Nat. Nanotechnol.* **16**, 1403–1412 (2021).
329. Dong, K. et al. Scalable electrophysiology of millimeter-scale animals with electrode devices. *BME Front.* **4**, 0034 (2023).
330. Gonzales, D. L. et al. Scalable electrophysiology in intact small animals with nanoscale suspended electrode arrays. *Nat. Nanotechnol.* **12**, 684–691 (2017).
331. Pratt, B., Deora, T., Mohren, T. & Daniel, T. Neural evidence supports a dual sensory–motor role for insect wings. *Proc. R. Soc. B Biol. Sci.* **284**, 20170969 (2017).
332. Yu, F. et al. Flexible microelectrode arrays to interface epicardial electrical signals with intracardial calcium transients in zebrafish hearts. *Biomed. Microdevices* **14**, 357–366 (2012).

333. Brenes, O. Invertebrate neurons as a simple model to study the hyperexcitable state of epileptic disorders in single cells, monosynaptic connections, and polysynaptic circuits. *Biophys. Rev.* **14**, 553–568 (2022).
334. Sahasrabudhe, A. et al. Multifunctional microelectronic fibers enable wireless modulation of gut and brain neural circuits. *Nat. Biotechnol.* **42**, 892–904 (2024).
335. Khatib, M. et al. Spiral neurostring: high-density soft bioelectronic fibers for multimodal sensing and stimulation. Preprint at *bioRxiv* https://doi.org/10.1101/2023.10.02.560482 (2023).
336. Du, P. et al. Recent progress in electrophysiology and motility mapping of the gastrointestinal tract using multi-channel devices. *J. R. Soc. N. Zeal.* **50**, 316–330 (2020).
337. Vu, M.-A. T. et al. A shared vision for machine learning in neuroscience. *J. Neurosci.* **38**, 1601–1607 (2018).
338. O'Neill, P. S. et al. A deep learning framework for automated and generalized synaptic event analysis. *eLife* **13**, RP98485 (2024).
339. Tankus, A., Solomon, L., Aharony, Y., Faust-Socher, A. & Strauss, I. Machine learning algorithm for decoding multiple subthalamic spike trains for speech brain–machine interfaces. *J. Neural Eng.* **18**, 066021 (2021).
340. Gupta, A., Vardalakis, N. & Wagner, F. B. Neuroprosthetics: from sensorimotor to cognitive disorders. *Commun. Biol.* **6**, 1–17 (2023).
341. Camacho-Conde, J. A., del Rosario Gonzalez-Bermudez, M., Carretero-Rey, M. & Khan, Z. U. Therapeutic potential of brain stimulation techniques in the treatment of mental, psychiatric, and cognitive disorders. *CNS Neurosci. Ther.* **29**, 8–23 (2023).
342. Famm, K., Litt, B., Tracey, K. J., Boyden, E. S. & Slaoui, M. A jump-start for electroceuticals. *Nature* **496**, 159–161 (2013).
343. Olofsson, P. S. & Bouton, C. Bioelectronic medicine: an unexpected path to new therapies. *J. Intern. Med.* **286**, 237–239 (2019).
344. Koutsouras, D. A., Malliaras, G. G. & Langereis, G. The rise of bioelectronic medicine. *Bioelectron. Med.* **10**, 19 (2024).
345. Plachta, D. T. T. et al. Blood pressure control with selective vagal nerve stimulation and minimal side effects. *J. Neural Eng.* **11**, 036011 (2014).
346. Valle, G. et al. Biomimetic intraneural sensory feedback enhances sensation naturalness, tactile sensitivity, and manual dexterity in a bidirectional prosthesis. *Neuron* **100**, 37–45.e7 (2018).
347. Wise, K. D. Silicon microsystems for neuroscience and neural prostheses. *IEEE Eng. Med. Biol. Mag.* **24**, 22–29 (2005).
348. Dartt, K. Principal component analysis for unit sorting: what it tells us and what it does not. *Plexon* https://plexon.com/blog-post/principal-component-analysis-for-unit-sorting/ (2024).
349. Ngo, H.-V. V., Born, J. & Klinzing, J. G. Protocol for spike-triggered closed-loop auditory stimulation during sleep in patients with epilepsy. *STAR Protoc.* **3**, 101505 (2022).
350. Rodionova, A., Bartocci, E., Nickovic, D. & Grosu, R. Temporal logic as filtering. In *Proc. 19th International Conference on Hybrid Systems: Computation and Control* 11–20 (Association for Computing Machinery, 2016).
351. Thiele, A. et al. Attention induced gain stabilization in broad and narrow-spiking cells in the frontal eye-field of macaque monkeys. *J. Neurosci.* **36**, 7601–7612 (2016).
352. Nowak, L. G. et al. Electrophysiological classes of cat primary visual cortical neurons in vivo as revealed by quantitative analyses. *J. Neurophysiol.* **89**, 1541–1566 (2003).
353. Peyrache, A. et al. Spatiotemporal dynamics of neocortical excitation and inhibition during human sleep. *Proc. Natl Acad. Sci. USA* **109**, 1731–1736 (2012).
354. Wojcik, D. The kinematics of spike trains. *Acta Phys. Pol. B* **49**, 2127 (2018).
355. Hubel, D. H. Tungsten microelectrode for recording from single units. *Science* **125**, 549–550 (1957).
356. Hodgkin, A. L. & Huxley, A. F. Action potentials recorded from inside a nerve fibre. *Nature* **144**, 710–711 (1939).
357. Zhang, L. A., Li, P. & Callaway, E. M. High-resolution laminar identification in macaque primary visual cortex using neuropixels probes. Preprint at *bioRxiv* https://doi.org/10.1101/2024.01.23.576944 (2024).
358. Inferring thalamocortical monosynaptic connectivity in vivo. *J. Neurophysiol.* https://journals.physiology.org/doi/full/10.1152/jn.00591.2020.
359. Perel, S., Schwartz, A. B. & Ventura, V. Automatic scan test for detection of functional connectivity between cortex and muscles. *J. Neurophysiol.* **112**, 490–499 (2014).
360. Bi, A. et al. Ectopic expression of a microbial-type rhodopsin restores visual responses in mice with photoreceptor degeneration. *Neuron* **50**, 23–33 (2006).
361. Neutens, P. et al. Dual-wavelength neural probe for simultaneous opto-stimulation and recording fabricated in a monolithically integrated CMOS/photonics technology platform. In *2023 International Electron Devices Meeting (IEDM)* 1–4 https://doi.org/10.1109/IEDM45741.2023.10413839 (IEEE, 2023).
362. Chen, F. D. et al. Development of wafer-scale multifunctional nanophotonic neural probes for brain activity mapping. *Lab. Chip* **24**, 2397–2417 (2024).
363. Kampasi, K. et al. Fiberless multicolor neural optoelectrode for in vivo circuit analysis. *Sci. Rep.* **6**, 30961 (2016).
364. Chen, F.-D. et al. Implantable neural probe system for patterned photostimulation and electrophysiology recording. In *2022 Conference on Lasers and Electro-Optics (CLEO)* 1–2 (Optica Publishing Group, 2022).
365. Lanzio, V. et al. Small footprint optoelectrodes using ring resonators for passive light localization. *Microsyst. Nanoeng.* **7**, 1–14 (2021).
366. Roszko, D. A. et al. Foundry-fabricated dual-color nanophotonic neural probes for photostimulation and electrophysiological recording. Preprint at *bioRxiv* https://doi.org/10.1101/2024.09.25.614961 (2024).
367. Vöröslakos, M. HectoSTAR µLED optoelectrodes for large-scale, high-precision in vivo opto-electrophysiology. *Adv. Sci.* https://onlinelibrary.wiley.com/doi/full/10.1002/advs.202105414 (2022).
368. Ko, E., Vöröslakos, M., Buzsáki, G. & Yoon, E. flexLiTE: flexible micro-LED integrated optoelectrodes for minimally-invasive chronic deep-brain study. Preprint at *bioRxiv* https://doi.org/10.1101/2022.08.05.503006 (2022).
369. Mohanty, A. et al. Reconfigurable nanophotonic silicon probes for sub-millisecond deep-brain optical stimulation. *Nat. Biomed. Eng.* **4**, 223–231 (2020).
370. Kampasi, K. et al. POEMS (polymeric opto-electro-mechanical systems) for advanced neural interfaces. *Mater. Lett.* **285**, 129015 (2021).
371. Segev, E. et al. Patterned photostimulation via visible-wavelength photonic probes for deep brain optogenetics. *Neurophotonics* **4**, 011002 (2017).
372. Beutel, H., Stieglitz, T. & Meyer, J. U. Microflex: a new technique for hybrid integration for microsystems. In *Proc. MEMS 98. IEEE. Eleventh Annual International Workshop on Micro Electro Mechanical Systems. An Investigation of Micro Structures, Sensors, Actuators, Machines and Systems* 306–311 (IEEE, 1998).
373. Roza, C. et al. Analysis of spontaneous activity of superficial dorsal horn neurons in vitro: neuropathy-induced changes. *Pflügers Arch. Eur. J. Physiol.* **468**, 2017–2030 (2016).


## Author contributions

Introduction (N.P.W., H.M., E.Y., T.S., T.D.H., A.B.S. and X.T.C.); Experimentation (N.P.W., M.V., M.Y.P., V.L., H.M., P.Z., E.Y., T.S., C.X., T.D.H., A.B.S. and X.T.C.); Results (N.P.W., M.V., D.S., M.Y.P., V.L., H.M., P.Z., E.Y., T.S., C.X. and T.D.H.); Applications (N.P.W., D.S., H.M., P.Z., E.Y., T.S., A.B.S. and X.T.C.); Reproducibility and data deposition (N.P.W., M.V., D.S., M.Y.P., V.L., H.M., P.Z., E.Y., T.S., T.D.H., A.B.S. and X.T.C.); Limitations and optimizations (N.P.W., M.V., D.S., M.Y.P., V.L., H.M., P.Z., E.Y., T.S., C.X., T.D.H., A.B.S. and X.T.C.); Outlook (N.P.W., D.S., M.Y.P., P.Z., T.S., C.X., A.B.S. and X.T.C.).

## Competing interests

P.Z. has equity in the start-up company Neuralthread, Inc., which seeks to commercialize flexible neural probe technology. C.X. is an inventor on intellectual property related to neurotechnology and a shareholder of Neuralthread, Inc. T.S. is a co-founder and scientific advisor of CorTec, GmbH and Neuroloop, GmbH. E.Y. is a co-founder of NeuroLight Technologies, a for-profit manufacturer of neurotechnology. The other authors declare no competing interests.

## Additional information

**Supplementary information** The online version contains supplementary material available at https://doi.org/10.1038/s43586-025-00399-7.

**Peer review information** *Nature Reviews Methods Primers* thanks Euan Brown, Torsten Bullmann and Vivian Rincón Montes for their contribution to the peer review of this work.